Cell Reports
Medicine

Article

Boosting NAD preferentially blunts Th17 inflammation via arginine biosynthesis and redox control in healthy and psoriasis subjects

Graphical abstract

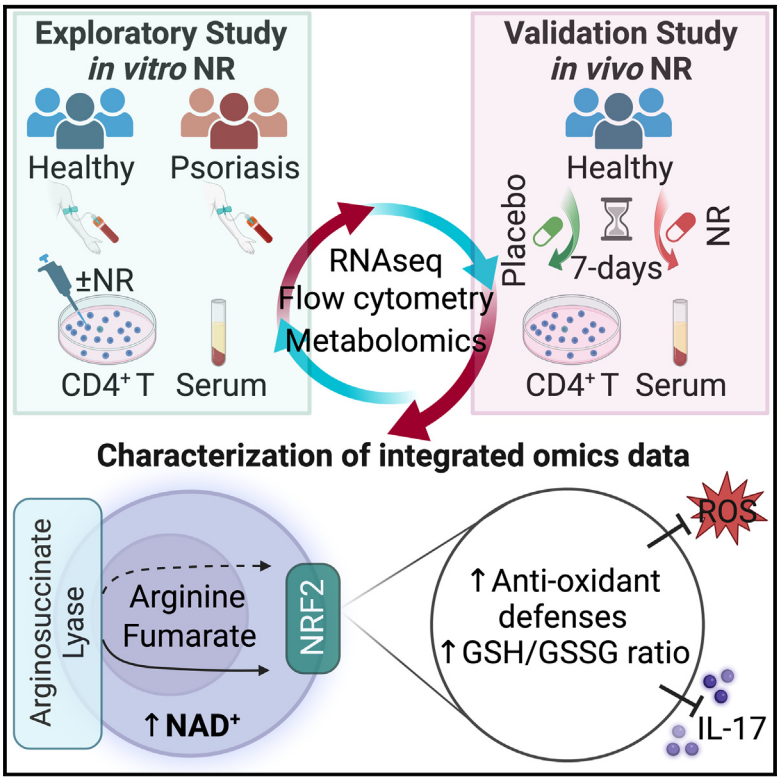

Highlights

- How NAD+ boosting blunts inflammation is poorly understood
- Integrated transcriptomics and metabolomics identify T cell regulatory pathways
- NAD+ increases arginine and fumarate biosynthesis
- These metabolites, via NRF2 signaling, blunt Th1 and Th17 immune responsiveness

Authors

Kim Han, Komudi Singh, Allison M. Meadows, ..., Rong Tian, Javier Traba, Michael N. Sack

Correspondence

sackm@nih.gov

In brief

Han et al. investigated NAD+-boosting effects on inflammation and found that nicotinamide riboside supplementation blunts Th1 and Th17 immune responsiveness in healthy volunteers and in psoriasis. Bioinformatics analysis uncovers that NAD+ boosting, via arginine and fumarate biosynthesis, activates NRF2. This transactivates antioxidant regulatory programs that blunt adaptive immune cell inflammatory signaling.

Han et al., 2023, Cell Reports Medicine *4*, 101157
September 19, 2023
https://doi.org/10.1016/j.xcrm.2023.101157

Cell Reports Medicine

CellPress
OPEN ACCESS

Article

Boosting NAD preferentially blunts Th17 inflammation via arginine biosynthesis and redox control in healthy and psoriasis subjects

Kim Han,[1] Komudi Singh,[1] Allison M. Meadows,[1,2] Rahul Sharma,[1] Shahin Hassanzadeh,[1] Jing Wu,[1] Haley Goss-Holmes,[1] Rebecca D. Huffstutler,[3] Heather L. Teague,[4] Nehal N. Mehta,[4] Julian L. Griffin,[2,5] Rong Tian,[6] Javier Traba,[1,7,8] and Michael N. Sack[1,2,9,*]

[1]Laboratory of Mitochondrial Biology and Metabolism, NHLBI, NIH, Bethesda, MD, USA
[2]Department of Biochemistry and Cambridge Systems Biology Centre, University of Cambridge, Cambridge, UK
[3]Cardiovascular Branch, NHLBI, NIH, Bethesda, MD, USA
[4]Laboratory of Cardiometabolic Disease and Inflammation, NHLBI, NIH, Bethesda, MD, USA
[5]The Rowett Institute, School of Medicine, Medical Sciences and Nutrition, Foresterhill Campus, Aberdeen, UK
[6]Mitochondria and Metabolism Center, Department of Anesthesiology and Pain Medicine, University of Washington School of Medicine, Seattle, WA, USA
[7]Instituto Universitario de Biología Molecular-UAM (IUBM-UAM), Departamento de Biología Molecular, Universidad Autónoma de Madrid, Madrid, Spain
[8]Centro de Biología Molecular Severo Ochoa, Consejo Superior de Investigaciones Científicas—Universidad Autónoma de Madrid (CSIC-UAM), Madrid, Spain
[9]Lead contact
*Correspondence: sackm@nih.gov
https://doi.org/10.1016/j.xcrm.2023.101157

SUMMARY

To evaluate whether nicotinamide adenine dinucleotide-positive (NAD^+) boosting modulates adaptive immunity, primary $CD4^+$ T cells from healthy control and psoriasis subjects were exposed to vehicle or nicotinamide riboside (NR) supplementation. NR blunts interferon γ (IFNγ) and interleukin (IL)-17 secretion with greater effects on T helper (Th) 17 polarization. RNA sequencing (RNA-seq) analysis implicates NR blunting of sequestosome 1 (*sqstm1/p62*)-coupled oxidative stress. NR administration increases *sqstm1* and reduces reactive oxygen species (ROS) levels. Furthermore, NR activates nuclear factor erythroid 2-related factor 2 (Nrf2), and genetic knockdown of *nrf2* and the Nrf2-dependent gene, *sqstm1*, diminishes NR amelioratory effects. Metabolomics analysis identifies that NAD^+ boosting increases arginine and fumarate biosynthesis, and genetic knockdown of argininosuccinate lyase ameliorates NR effects on IL-17 production. Hence NR via amino acid metabolites orchestrates Nrf2 activation, augments $CD4^+$ T cell antioxidant defenses, and attenuates Th17 responsiveness. Oral NR supplementation in healthy volunteers similarly increases serum arginine, *sqstm1*, and antioxidant enzyme gene expression and blunts Th17 immune responsiveness, supporting evaluation of NAD^+ boosting in $CD4^+$ T cell-linked inflammation.

INTRODUCTION

Nicotinamide (NAM) adenine dinucleotide (NAD) is an essential co-enzyme and metabolic substrate for innumerable cellular processes to maintain homeostasis and energy metabolism.[1] Cellular NAD^+ levels are determined by the balance between NAD consumption, *de novo* synthesis, and recycling through the NAD salvage pathway. Disruption in this balance results in reduced NAD levels in distinct organs, which is evident in aging,[2,3] obesity-induced diabetes,[4] heart failure with preserved ejection fraction,[5] and inflammatory conditions.[6] Conversely, excessive NAD^+ may lead to cancer growth,[1] disruption in stem cell function,[7] augmentation of immune cell proliferative function,[7] and enhancement of tumor-infiltrating lymphocyte (TIL) function.[8,9] Despite this potential divergent spectrum of effects and given the potential salutary effects of NAD augmentation against numerous metabolic and degenerative diseases, investigators have begun to explore the effects of NAD salvage pathway intermediates as supplements for targeted diseases and with aging. Intermediates in the NAD salvage pathway, including NAM, NAM mononucleotide (NMN), and NAM riboside (NR), have been employed to assess their role in biology and in disease pathophysiology. In mouse models, NAM has been shown to reduce autoimmune encephalitis[10] and ameliorate genetic disrupted $CD4^+$ T cell inflammation.[11] Similarly, NMN has shown ameliorative effects against obesity, diabetes,[4] neurodegeneration, cerebral and cardiac ischemia, and kidney damage. In parallel, NR supplementation augments $CD8^+$ TIL

function[9] and shows beneficial effects against murine models of type 2 diabetes.[12] In humans, studies to date suggest that NMN may appear to have numerous beneficial effects, and a question has been posited as to whether NR may have tissue-specific rather than systemic effects.[1]

Given that inflammation and/or perturbed immune responses are common underpinnings of diseases linked to NAD depletion, the role of these supplements in immune cell function are being actively pursued.[13] For example, NMN suppressed gene signatures of age-associated murine adipose tissue inflammation,[14] and NR reduced neuroinflammation in a murine model of Alzheimer's disease.[15] The role of NR on the human immune system is further evident where NR depressed inflammatory cytokines in older men,[16] reduced the inflammasome in human monocytes,[17] blunted monocytic type I interferon (IFN) signaling,[18] diminished inflammation in peripheral blood mononuclear cells (PBMCs) in heart failure subjects,[19] and reduced systemic and neuro-inflammation in Parkinson disease.[20] Moreover, coronavirus infection was recently shown to induce an IFN response that depressed cellular NAD^+ in a manner that was opposed by supporting NAD status.[21] Given these findings, and the potential use of the NAD^+ booster NR as a therapeutic supplement, further study into the regulatory mechanisms underpinning the NR effect on immune cells is warranted. Because prior studies have predominantly focused on innate immune effects, this study was directed at exploring adaptive immunity. To initiate this study, we evaluated *ex vivo* NR supplementation on primary $CD4^+$ T helper (Th) cell extracted from healthy volunteers. Here we uncovered that NAD^+ boosting blunted Th1 and Th17 immune responsiveness, with the more robust regulatory effects on Th17 polarization. To link the role of NAD^+ boosting to a disease process linked to increased Th1 and Th17 activation, we then investigated NR effects on the inflammatory disease psoriasis. Psoriasis affects 2–3% of the US population. In addition to its skin and joint manifestations, psoriasis predisposes to premature cardiovascular co-morbidities in part through immune activation and systemic inflammation-induced atherosclerosis.[22,23] The skin-initiated immune activation through non-professional immune cells, including keratinocytes and fibroblasts, initiates and amplifies innate and adaptive immune activity of monocytes/macrophages, neutrophils and their subsets (low-density granulocytes), and effector T cells (predominantly Th1 and Th17 subsets),[24,25] which concurrently exacerbate local disease and initiate systemic sterile inflammation. The centrality of immune activation in psoriasis is reinforced by the therapeutic efficacy of anti-tumor necrosis factor alpha (anti-TNF-α) and anti-interleukin (IL)-17 therapy.[26–28]

The major subsequent findings from this study show: (1) *ex vivo* NR supplementation blunted Th1 and Th17 immune-responsiveness in $CD4^+$ T cells from healthy volunteers and from patients with mild-moderate psoriasis; (2) $CD4^+$ T cell RNA sequencing (RNA-seq) analysis from these study subjects identifies that commonly expressed differentially expressed (DE) genes in response to NR augment antioxidant defense pathways; (3) bioinformatics protein-protein interaction analysis of these DE genes implicated the sequestosome 1 (SQSTM1)-NRF regulatory pathway in coordinating these effects; (4) genetic, pharmacologic, and biochemical analysis confirmed that NR upregulated both *sqstm1* and nuclear factor erythroid 2-related factor 2 (Nrf2), and that these pathways were instrumental in reducing cellular reactive oxygen species (ROS) and in blunting Th17 responsiveness; (5) metabolomics analysis identified that NR augmented the arginine biosynthesis pathway, and that the generation of arginine and fumarate, established inducers of Nrf2 activity,[29–31] replicated the immunoregulatory effects of NR; and finally, (6) a pilot *in vivo* supplementation study in healthy volunteers showed that NR blunted Th17 gene regulation and immune responsiveness and induced antioxidant gene expression in parallel with increasing serum arginine levels.

RESULTS

NR supplementation blunts $CD4^+$ Th cell responsiveness in volunteers with and without psoriasis

To initiate this study, we extracted primary human $CD4^+$ T cells from healthy volunteers to evaluate NAD^+ boosting on Th cell activation. Following *ex vivo* vehicle or NR supplementation and activation, flow cytometry showed that Th1 ($Tbx21^+IFN\gamma^+$) and Th17 ($Rorc^+IL17^+$) polarization were blunted by NR, whereas markers of the Th2 lineage ($Gata3^+IL4^+$) were unchanged (Figure 1A). In parallel, at the transcript level in response to specific Th cell polarization, NR blunted canonical Th17 transcriptional activator *rorc* levels in Th17 cells (Figure S1A). In contrast, NR had no effect on the expression of the Th1 transcription factor *tbx21* in Th1 and increased the Th2 transcription factor *gata3* in Th2 polarized cells, respectively (Figure S1A). To then evaluate whether NR has an immunomodulatory effect on Th cell responsiveness in inflammation, we obtained primary $CD4^+$ T cells from age- and gender-matched control and psoriasis subjects (Figure 1B) and subjected them to NR administration and T cell receptor (TCR) activation *in vitro*. Because the inflammatory skin disease psoriasis is linked to Th1 and Th17 activation, we measured the effect of NR supplementation on IFNγ and IL-17 secretion. In TCR-activated $CD4^+$ T cells and specific lineage polarized cells (Th1 and Th17), the levels of IFNγ and IL-17 were significantly blunted by NR in both groups (Figures 1C and 1D). In alignment with the initial healthy volunteer subject transcription factor expression levels (Figure S1A), the NR dampening effect was more robust for IL-17 rather than IFNγ when assessing relative changes in Th0, Th1, and Th17 cells (Figures S1B and S1C). Interestingly, this NR-mediated reduction in cytokine levels was evident across the spectrum of disease severity measured by the psoriasis area and severity index (PASI) (Figure S1D).

To explore the regulatory mechanisms, we performed RNA-seq on $CD4^+$ T cells isolated from these healthy and psoriatic subjects in the presence or absence of NR, and the complete database is available in NCBI's Gene Expression Omnibus (GEO: GSE237556). 549 and 1,160 transcripts levels, respectively, were DE in TCR-activated $CD4^+$ T cells from healthy control and psoriasis groups by NR compared with vehicle (Figure S1E), and principal-component (PC) analysis (PCA)

CellPress
OPEN ACCESS

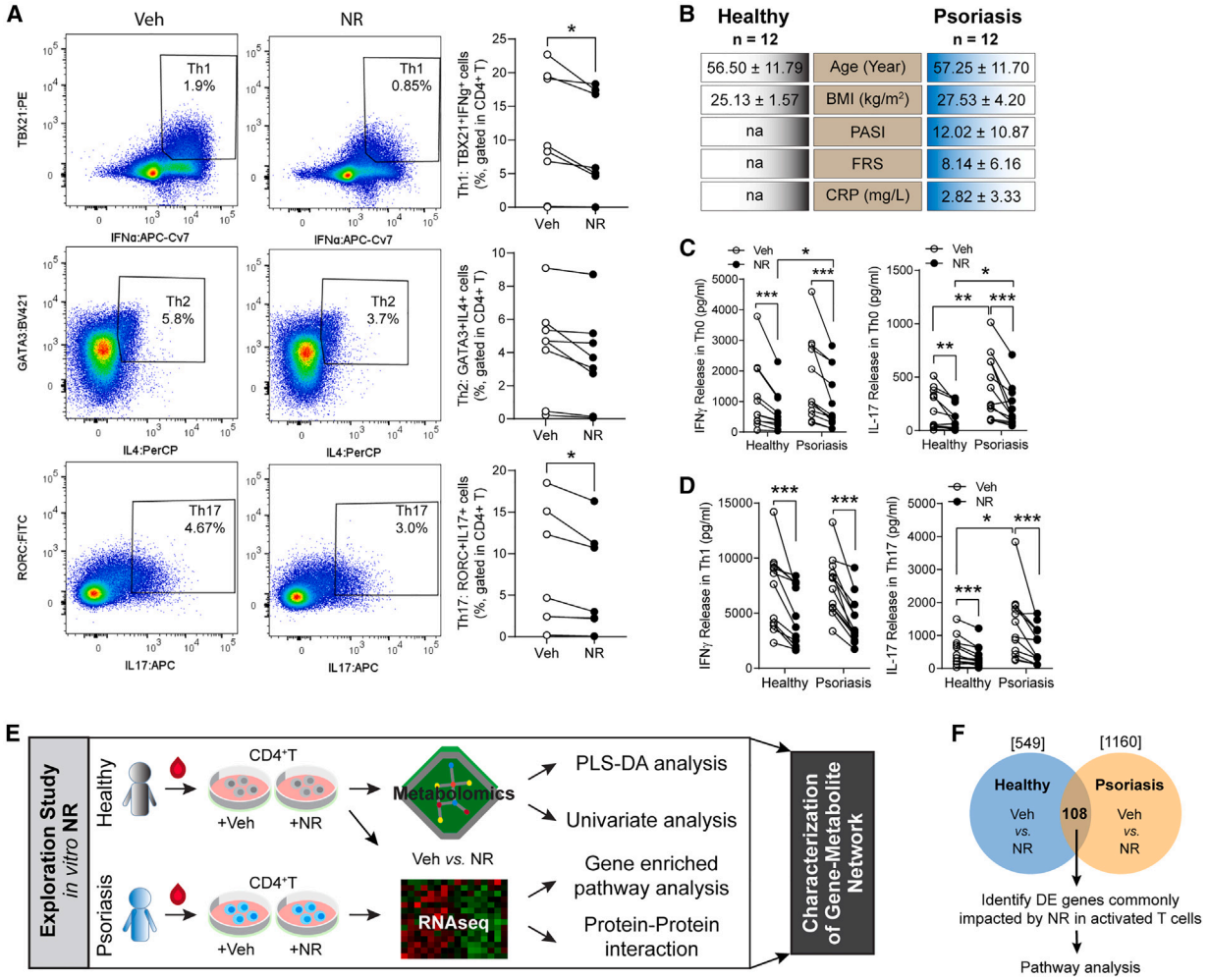

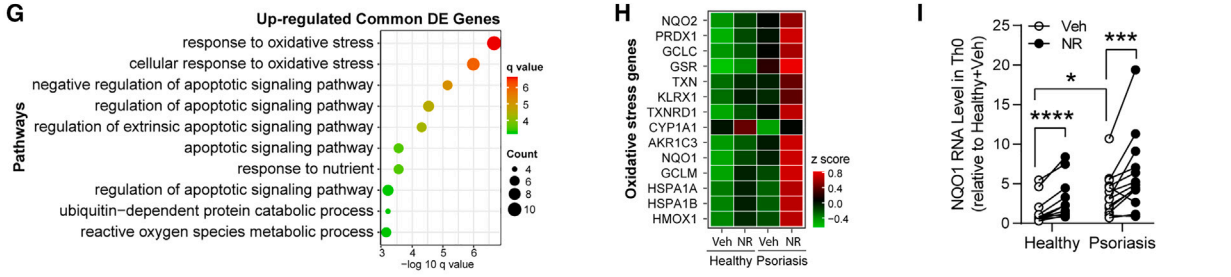

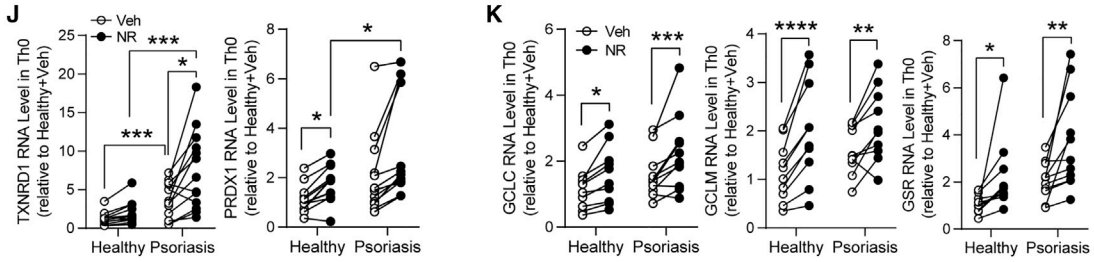

(legend on next page)

confirmed NR as the PC (PC1 axis) driving these DE genes (Figure S1F; Tables S1 and S2). To uncover NR-regulated genes in control and psoriasis subjects, we examined intersecting DE genes comparing vehicle with NR-supplemented activated CD4$^+$ T cells by pathway analyses. This approach is schematized in Figure 1E. The top 10 enriched pathways of activated cells in both groups show that NR regulated oxidative stress, T cell activation, and neutrophil activation, respectively (Figures 1G–1J). A total of 108 DE genes were commonly impacted by NR in both groups and of these, 39 increased and 69 showed reduced transcript levels (Figure 1F). Pathway analysis of these common upregulated and downregulated genes implicated NR in the response to oxidative stress, to protein catabolism, and to the negative regulatory effect on apoptosis and on RNA processing (Figures 1G and S1K). A heatmap of upregulated genes by NR in healthy and psoriasis subjects showed that NR robustly upregulated antioxidative response genes (Figure 1H). To explore the transcripts induced by NR, we performed qRT-PCR analysis to measure the mRNA levels linked to ROS detoxification (*nqo1*), ROS elimination (*txnrd1* and *prdx1*), and glutathione synthesis (glutamate-cysteine ligase catalytic subunit [*gclc*], glutamate-cysteine ligase modifier subunit [*gclm*], and *gcr*). These were similarly upregulated in response to NR in the control and psoriasis cohorts (Figures 1I–1K). Transcript levels encoding genes linked to the oxidative degradation of heme groups (*hmox1*) and to xenobiotic metabolism (*cyp1a1*) were similarly induced by NR (Figure S1L).

NR blunted ROS production and reduced lipid peroxidation products in CD4$^+$ T cells in a glutathione-dependent manner

To evaluate the functional effect of NR on ROS production in CD4$^+$ T cells, we measured mitochondrial superoxide levels and whole-cell ROS activity. Consistent with the RNA-seq data, in both cohorts NR blunted ROS levels and mitochondrial ROS activity in activated Th0 cells (Figures 2A and 2B). In parallel, NR blunted lipid peroxidation products (Figure 2C) and augmented the antioxidant capacity in healthy and psoriatic Th0 cells (Figure 2D). Interestingly, vehicle treatment uncovers that antioxidant capacity is significantly lower in psoriasis than in controls (Figure 2D). Furthermore, following CD4$^+$ T cell polarization into the Th17 cell lineage, NR again blunted ROS activity in the control and psoriatic groups (Figures 2E and 2F). To explore the mechanisms orchestrating these immunomodulatory effects, we performed all subsequent experiments in either activated non-polarized CD4$^+$ T cells (Th0) or cells polarized to the Th17 lineage.

To further assess the NR effect, Kyoto Encyclopedia of Genes and Genomes (KEGG) analysis showed enrichment of upregulated DE genes in the glutathione metabolism (Figures S2A and S2B). In parallel, the ratio of reduced glutathione (Gsh) to oxidized glutathione disulfide (Gssg) glutathione was induced by NR in Th0 and Th17 CD4$^+$ T cells (Figures 2G and 2H). Furthermore, transcript levels encoding genes driving glutathione synthesis, including *gclc* and *gclm*, and in the reduction of Gssg to Gsh, i.e., glutathione-disulphide reductase (*gsr*), were all significantly increased in Th0 cells from healthy control and psoriasis subjects (Figure 1K). Subsequent knockdown (KD) of these genes abrogated the blunting effect of NR on IL-17 secretion and on ROS levels assayed with 2′,7′-dichlorofluorescin diacetate (DCFDA) and MitoSOX fluorescence in Th0 and Th17 polarized cells (Figures 2I–2N). KD efficiency of the respective genes is shown in Figure S2C. As expected, KD of these enzymes abolished the NR effect on increasing cellular glutathione levels and antioxidant capacity (Figures S2D and S2E).

The antioxidant and anti-inflammatory effects of NR are Nrf2 dependent

To explore the putative mechanism orchestrating these effects, we analyzed the overlapping NR-responsive DE genes from

Figure 1. NR supplementation blunts CD4$^+$ Th cell responsiveness in healthy volunteers and in psoriasis

(A) Representative flow cytometry plots of activated CD4$^+$ T cells with vehicle and NR treatment. The dot-line plots show gated Th0 cell population (percentiles). Th1, Tbx21$^+$IFNγ^+; Th2, Gata3$^+$IL4$^+$; Th17, Rorc$^+$IL-17$^+$ (n = 8 individuals).

(B) Characteristics of subjects enrolled in this study (male, n = 12 per group). Data represent mean ± standard deviation (SD).

(C) IFNγ and IL-17 release in activated CD4$^+$ T cells isolated from psoriatic and healthy subjects (male, n = 12/group). CD4$^+$ T cells activated with 0.5 mM NR and 10% autologous serum for 3 days by anti-CD3 and anti-CD28.

(D) IFNγ and IL-17 release in differentiated CD4$^+$ T cells from psoriatic and healthy subjects (n = 12/group). Differentiation supplement: Th1 (STEMCELL Technologies) and Th17 (R&D Systems).

(E) Schema describing exploration study undertaken to assess mechanisms of *in vitro* NR-mediated immunomodulation. Study included CD4$^+$ T cells isolated from healthy and psoriatic participants followed by NR treatment *in vitro*. Subsequent metabolomics and gene-expression profiling datasets were used to characterize gene-metabolite networks.

(F) Venn diagram showing healthy vs. psoriasis datasets used to identify NR-modulated genes specifically impacted in activated CD4$^+$ T cells for 3 h (n = 8 subjects/group). The 108 common DE genes regulated by NR were subjected to clusterProfiler pathway enrichment analysis.

(G) Dot plot of clusterProfiler pathway from 39 upregulated genes out of a total of 108 common DE genes. The x axis represents negative log10-transformed q values, and the dot-plot color was scaled to transformed q values. The size of the dot was scaled to number of genes overlapping with the indicated pathway on the y axis.

(H) Heatmap of Gene Ontology (GO) response to oxidative stress genes in 108 common DE genes.

(I–K) Quantitative RT-PCR analysis of the mRNA levels linked to ROS detoxification (I, *nqo1*), ROS elimination (J, *txnrd1* and *prdx1*), and glutathione synthesis (K, *gclc, gclm*, and *gsr*) in activated CD4$^+$ T cells from healthy and psoriatic subjects. NR was administrated to the CD4$^+$ T cells during TCR activation for 3 h (n = 12 subjects/group). Data point of each subject shown as dots (c, d, i, j, and k). The p values for comparisons of two groups calculated using unpaired two-tailed Student's t test (healthy vs. psoriasis) or paired two-tailed Student's t test (vehicle vs. NR). *p < 0.05, **p < 0.01, ***p < 0.001.

BMI, body mass index; CRP, C-reactive protein; FRS, Framingham risk score; na, not applicable; NR, nicotinamide riboside; PASI, psoriasis area and severity index.

CellPress
OPEN ACCESS

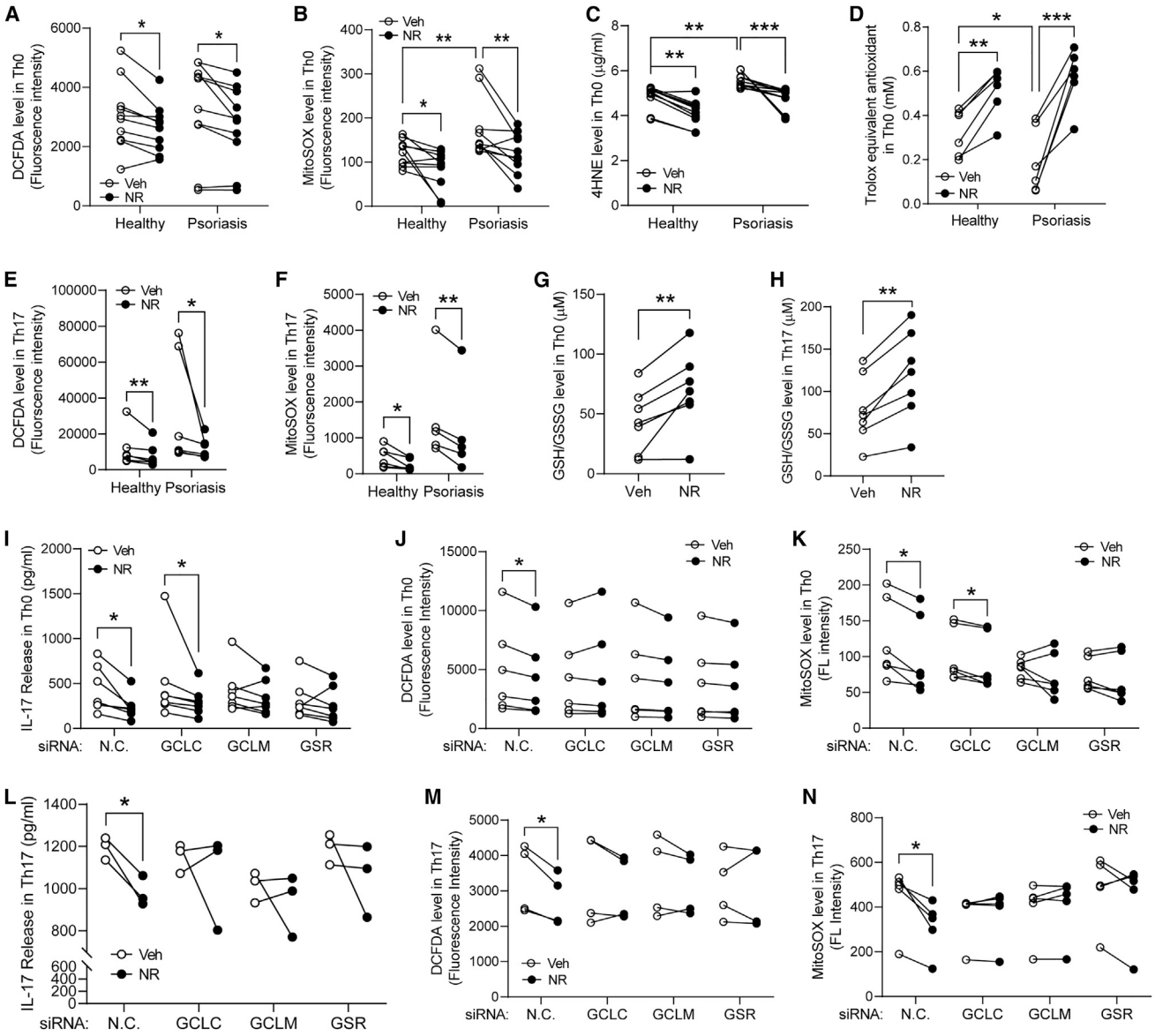

Figure 2. NR blunts ROS production and reduces lipid peroxidation products in CD4$^+$ T cells in a glutathione-dependent manner

(A and B) Cellular ROS level (A, dichlorodihydrofluorescein diacetate [DCFDA]) and mitochondrial ROS level (B, MitoSOX) in activated CD4$^+$ T cells isolated from psoriatic and healthy subjects (DCFDA, n = 6/group; MitoSOX, n = 5–8/group). CD4$^+$ T cells activated with 0.5 mM NR and 10% autologous serum for 3 days and anti-CD3 and anti-CD28.

(C) 4-HNE (4-hydroxynonenal, lipid peroxidation) level in activated CD4$^+$ T cells from healthy and psoriatic subjects in the presence of vehicle or NR.

(D) Trolox equivalent antioxidant capacity of NR was measured in activated CD4$^+$ T cells (n = 6 subjects/group).

(E and F) Cellular ROS (E) and mitochondrial ROS level (F) in differentiated Th17 cells. CD4$^+$ T cells isolated from psoriatic and healthy subjects differentiated with specific differentiation media in 10% autologous serum for 3 days with TCR activation ± NR (DCFDA, n = 6/group; MitoSOX, n = 5–8/group). Th17 differentiation media, 20 ng/mL rIL-6, 2.5 ng/mL transforming growth factor β (TGF-β), 10 μg/mL anti-IL-4, and 10 μg/mL anti-IFNγ.

(G and H) The ratio of GSH/GSSH level in activated (G) and Th17-differentiated CD4$^+$ T cells (H) with NR for 3 days (n = 7).

(I and L) IL-17 release following knockdown (KD) of glutathione-regulated genes (*gclc, gclm*, or *gsr*) in activated Th0 (I, n = 12) and Th17 cells (L, n = 3). CD4$^+$ T cells activated with 0.5 mM NR following siRNA delivery.

(J, K, M, and N) Relative cellular ROS level (J and M) and mitochondrial ROS level (K and N) level in *gclc*, *gclm*, or *gsr* siRNA Th0 (n = 6) and Th17 cells (n = 4). CD4$^+$ T cells were differentiated with Th17 differentiation media.

Data point of each subject shown as dots in all figure panels. The p values for comparisons of two groups calculated using unpaired two-tailed Student's t test (healthy vs. psoriasis) or paired two-tailed Student's t test (vehicle vs. NR), or by ANOVA for multiple comparisons. *p < 0.05, **p < 0.01, ***p < 0.001. FL, fluorescence.

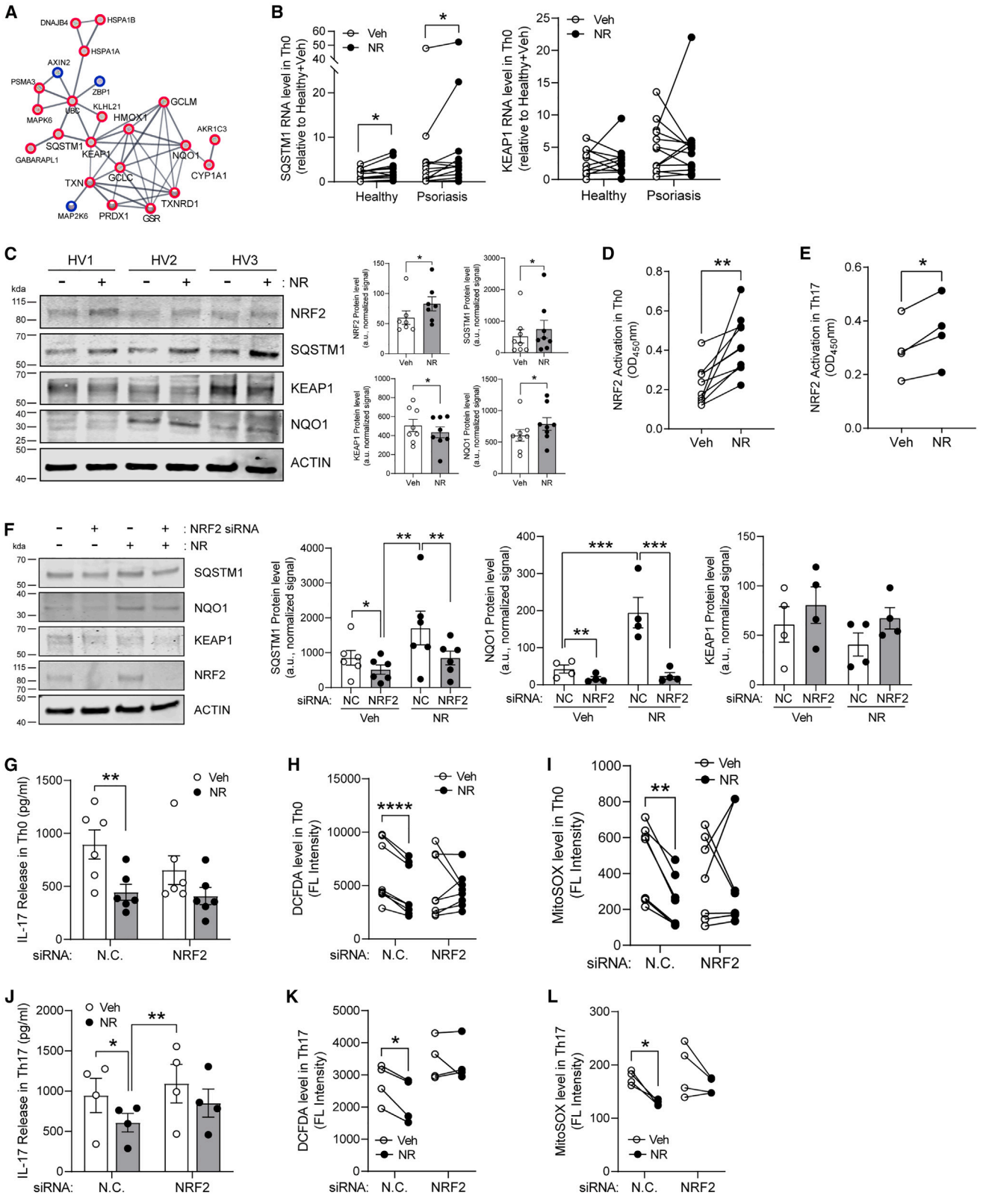

(legend on next page)

healthy and psoriasis cohorts for curated protein-protein interactions (PPIs) (Figure 3A). Notably, the pathway linked with oxidative stress pathways included changes in expression of *sqstm1*/p62 and Kelch-like ECH-associated protein 1 (*keap1*). An established mechanism whereby Sqstm1 modulates ROS regulatory transcript levels and ROS biology is via sequestration of Keap1 to enable Nrf2 transactivation of ROS regulatory genes.[32] At the same time, *sqstm1* is induced by Nrf2 via binding to its antioxidant response element (ARE).[33] qRT-PCR assessment of transcript levels encoding *sqstm1*, but not *keap1*, aligned with this RNA-seq bioinformatics analysis (Figure 3B). Furthermore, NR increased the protein expression of Nrf2 and Sqstm1 with a modest reduction in Keap1 levels (Figure 3C).

To evaluate whether NRF2 is an important NR-responsive regulatory factor in immunomodulation, we assayed NRF2 activity in Th0 and Th17 cells. In both lineages, NR increased NRF2 activity (Figures 3D and 3E). Interestingly, psoriatic CD4$^+$ T cells had less NRF2 binding activity compared with healthy Th0 cells (Figure S3A). To genetically interrogate this pathway, we depleted Nrf2 by small interfering RNA (siRNA) (Figures 3F and S3B). Nrf2 KD abolished the NR IL-17 blunting effect in Th0 and Th17 cells (Figures 3G and 3J) and the effects on DCFDA and MitoSOX levels in Th17 cells (Figures 3H, 3I, 3K, and 3L). The overexpression of Nrf2 had the opposite effect (Figures S3C–S3F). In parallel, the Nrf2 activator dimethyl fumarate (DMF) and the Nrf2 inhibitor ML385 had opposing effects, with DMF paralleling the effects of NR in blunting IL-17 release and ML385 by increasing cytokine secretion (Figures S3G–S3J). Nrf2 KD similarly blunted transcript levels of *sqstm1* and *nqo1* and the antioxidant defense genes *nqo1* and *gclm* (Figures 3F and S3K). However, *keap1* expression was not altered (Figures 3F and S3K).

Because *sqstm1* is a canonical NRF2 target, its levels were manipulated by siRNA and overexpression to assess these effects on Th17 biology. The interrelated regulation of these two proteins was confirmed where KD of Sqstm1 blunted Nrf2 and Nqo1 protein levels (Figures 4A and S4A). In parallel with this, KD of Sqstm1 abolished the blunting effects of NR on IL-17 release, DCFDA, and MitoSOX (Figures 4B–4G). Conversely, overexpression of *sqstm1* per se did not constitutively reduce the release of IL-17 or change the levels of DCFDA, although they did have a significant effect in reducing MitoSOX levels in Th0 cells (Figures S4B–S4D).

The CD4$^+$ T cell immunomodulatory effect of NR is dependent on cellular NAD$^+$ levels

It is likely that NR boosts redox enzyme reactions and/or decreases inflammatory cytokines via modulation of NAD-consuming pathways. Prior to assessing this, we first evaluated whether these NR effects are NAD$^+$ dependent, increasing NAD levels in CD4$^+$ T cells via pharmacologic inhibition of NAD-consuming pathways using inhibitors of PARP enzymes and Cd38 and via genetic depletion of NAD-consuming proteins Cd38 and Sarm1.[34,35] Inhibition of PARPs with rucaparib and Cd38 activity by compound 78c both mirrored the effect of NR and rescued IL-17 release and ROS levels (Figures 5A–5F). Similarly, siRNA KD of Cd38 and Sarm1 replicated the blunting effects on IL-17 levels, DCFDA, and MitoSOX in Th0 (Figures 5G–5I) and Th17 cells (Figures 5J–5L) and increased protein expression of NRF2 and SQSTM1 (Figures 5M and 5N). Interestingly, and consistent with inflammation in psoriasis, the NAD/NADH ratio was reduced in psoriatic Th0 cells compared with the healthy group (Figure S5A). In parallel, transcript levels of *cd38*, *sarm1*, *parp4*, and *parp12*, which promote NAD breakdown and consumption, were concordantly upregulated in the psoriatic subjects (Figure S5B). Together, these data support that NAD consumption is probably increased in psoriasis, and that NAD$^+$ boosting is both necessary and sufficient to blunt Th17 immune cell responsiveness.

Metabolomics analysis implicates CD4$^+$ T cell arginine and fumarate biosynthesis as mediators of NR's immunomodulatory effect

Earlier in these studies, it was noted that the fumarate methyl ester DMF could replicate the effect of NR in blunting IL-17 release (Figures S3F and S3G). A question that arose is whether NR modulated the fumarate synthesis in CD4$^+$ T cells. To pursue this concept, we performed steady-state metabolomics analysis in activated Th0 and Th17 cells. Orthogonal partial least squares discrimination analysis showed that the changes in metabolites were distinct in both different lineages in response to NR (Figure 6A). Variables of importance in prediction (VIP) analysis with a score >1.5 were assessed in the Th0 and Th17 cells and uncovered that distinguishing metabolites between NR and vehicle was similar in both lineages (Figures 6B, S6A, and S6B; Table S3). Interestingly, these included numerous NAD$^+$ intermediates, as well as amino acid intermediates, in the glutamine and arginine metabolic pathways. The top 10 pathways of these

Figure 3. The antioxidant and anti-inflammatory effects of NR are dependent on NRF2

(A) 108 common DE genes shown in Figure 1F were used to build a protein-protein interactome. Each node depicts a gene and its potential interaction with other genes, represented by the edges (gray color lines). Gene-expression fold-change information is overlaid on the node, upregulated by NR (red border) and downregulated by NR (blue border). Healthy vs. psoriasis datasets were used to identify NR-modulated genes specifically impacted by 3 h of CD4$^+$ T cell activation (n = 8 subjects/group).

(B) Quantitative RT-PCR analysis of *sqstm1* and *keap1* shown in PPI analysis in activated CD4$^+$ T cells from healthy and psoriatic subjects (n = 12 subjects/group).

(C) Protein expression and quantification of Nrf2, Sqstm1, Keap1, and Nqo1 following NR treatment of activated cells (n = 8).

(D and E) NRF2 activity in Th0 (D, n = 7) and Th17 following NR (E, n = 4). Active Nrf2 is present in the nuclear extract binding to immobilized Nrf2 consensus binding oligonucleotide (5′-GTCACAGTGACTCAGCAGAATCTG 3′).

(F) Protein expression of Sqstm1, Nqo1, and Keap1 in *nrf2*-KD CD4$^+$ T cells following NR (n = 4–6).

(G and J) IL-17 release in *nrf2*-KD CD4$^+$ T cells (G, n = 6) and Th17 cells with NR (J, n = 4).

(H, I, K, and L) Cellular ROS and mitochondrial ROS in *nrf2* KD Th0 (H and I, n = 7–8) and Th17 cells with NR (K and L, n = 4).

The p values for comparisons of two groups calculated using unpaired two-tailed Student's t test (NC vs. *nrf2* KD) or paired two-tailed Student's t test (vehicle vs. NR), or by ANOVA for multiple comparisons. *p < 0.05, **p < 0.01, ***p < 0.001. A.U., arbitrary units; N.C., negative control. Histograms represent mean ±SEM.

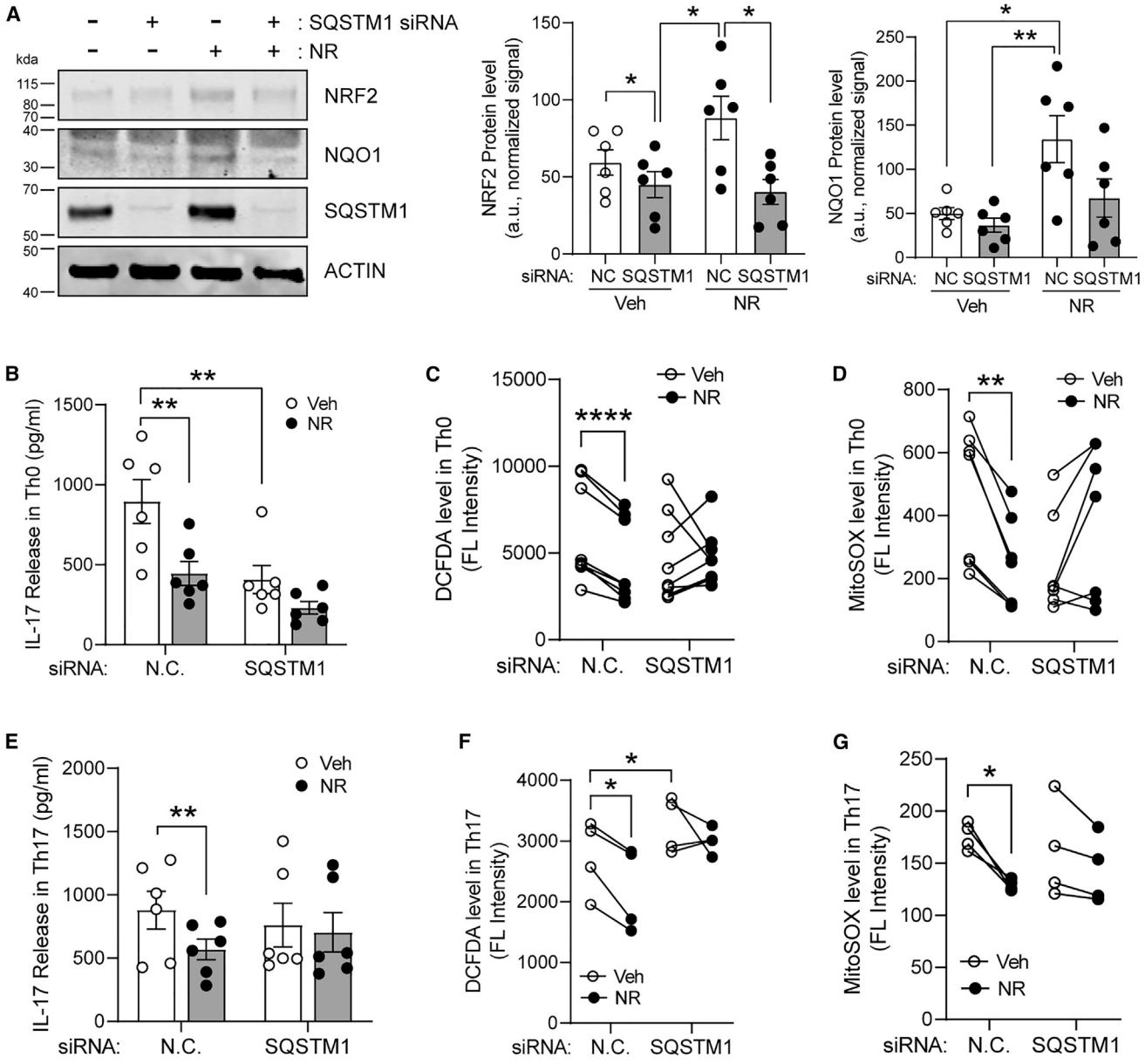

Figure 4. The antioxidant and anti-inflammatory effects of NR are dependent on NRF2-binding proteins

(A) Protein expression and quantification of Nrf2 and Nqo1 following *sqstm1* siRNA in Th0 cells (n = 6).

(B and E). IL-17 release from *sqstm1*-KD $CD4^+$ T cells (B, n = 6) and Th17 cells following NR (E, n = 6).

(C, D, F, and G). Cellular ROS and mitochondrial ROS in *sqstm1* KD cells following NR (C and D, n = 6) and in Th17 differentiated cells (*sqstm1* siRNA delivery plus NR) (F and G, n = 4). The p values for comparisons of two groups were calculated using unpaired two-tailed Student's t test (NC vs. *sqstm1* KD) or paired two-tailed Student's t test (vehicle vs. NR), or by ANOVA for multiple comparisons.

All data are represented as mean ± SEM. *p < 0.05, **p < 0.01, ***p < 0.001. Histograms represent mean ±SEM.

metabolites enriched in arginine biosynthesis and glutathione metabolism pathways. Additional pathways suggested that changes in other amino acid levels may also contribute to the effect of NR, including aspartate (Figures 6C and S6C). Furthermore, levels of arginine and fumarate were elevated in both Th0 and Th17 cells in response to NR supplementation (Figure 6D). However, the metabolites (ornithine, citrulline, and argininosuccinic acid) upstream of arginine biosynthesis were not altered by NR (Figure S6D). In parallel with the DMF effect in $CD4^+$ T cells, L-arginine supplementation similarly blunted IL-17 release and ROS levels (Figures S6E–S6G). Arginine supplementation similarly increased Nrf2 activity and Nrf2 and Sqstm1 protein levels (Figures S6H and S6I). Interesting, in the context of the urea cycle, the biosynthesis of fumarate requires aspartate and concurrently generates arginine, with argininosuccinate lyase (ASL) being the major enzyme for arginine and fumarate

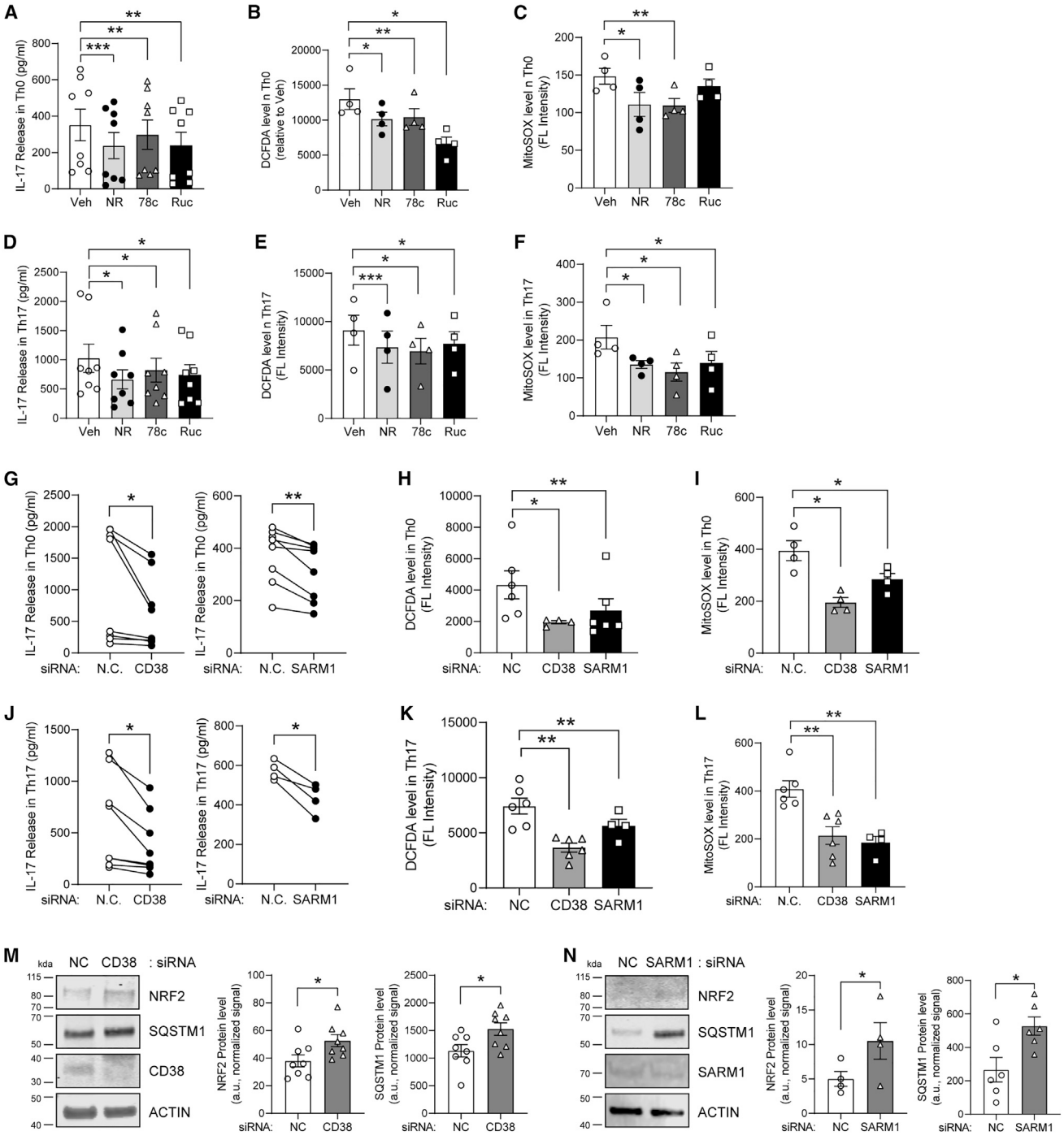

Figure 5. The CD4$^+$ T cell immunomodulatory effect of NR is dependent on cellular NAD$^+$ levels

(A) IL-17 release in response to Compound 78c (78c) to inhibit CD38 or rucaparib (Ruc) to inhibit PARPs (n = 8) in CD4$^+$ T cells.

(B and C) Cellular ROS (B) and mitochondrial ROS (C) following 78c or Ruc (n = 4).

(D) IL-17 release following 78c or Ruc in Th17 cells (n = 8).

(E and F) Cellular ROS (E) and mitochondrial ROS (F) following 78c or Ruc in Th17 cells (n = 4).

(G) IL-17 release in *cd38*- or *sarm1*-KD CD4$^+$ T cells (n = 8).

(H and I) ROS (H) and mitochondrial ROS (I) in *cd38*- or *sarm1*-KD cells (n = 4).

(J) IL-17 release in *cd38*- or *sarm1*-KD Th17 cells (n = 4–8).

(legend continued on next page)

synthesis. To evaluate whether this metabolic pathway was involved, siRNA targeting ASL was performed. Following *asl* KD, the NR effect on blunting IL-17 and ROS levels was abrogated (Figures 6E–6G and 6I–6K). In parallel, KD of *asl* blunted Nrf2 activity and the transcript levels of genes encoding Nqo1 and Gclc (Figures S6J and S6K). Together, these data support that NR-mediated biosynthesis of arginine and fumarate, with subsequent transactivation of Nrf2 and its canonical targets, blunted CD4$^+$ T cell IL-17 production.

In vivo supplementation of NR in healthy volunteers recapitulated *ex vivo* NR effects on CD4$^+$ T cell activation

Finally, whether the supplementation of NR *in vivo* orchestrates the same effects remained unknown. To test this, we used primary CD4$^+$ T cells from a prior placebo-controlled study where NR was found to blunt immune responsiveness in monocytes.[18] As an exploratory endpoint in that study, we extracted CD4$^+$ T cells by negative selection from placebo and NR (500 mg twice daily) study subjects after 7 days of supplementation (Figure S7A). Datasets of gene-expression profiling and metabolomics were employed to assess whether the pathways and networks identified in the exploratory study (Figure 1E) were operational *in vivo*. The schema of this validation study is shown in Figure 7A. CD4$^+$ T cells were isolated from these subjects consuming placebo or NR, and RNA was extracted and prepared for RNA-seq analysis (Figure S7B). The subject characteristics and the response to NR supplementation with respect to levels of NAD$^+$ metabolites were described previously.[18] Flow cytometry from PBMCs following NR *in vivo* supplementation mirrored the *ex vivo* studies, showing that NAD$^+$ boosting reduced Th1 and Th17 molecular signatures in CD4$^+$ gated T cells (Figure 7B) with a greater effect on Th17 (Figure 7C). This finding was supported by the direct cytometric analysis of antibodies targeting IFNγ, IL-4, and IL-17 in CD25$^+$HLADR$^+$ activated cells (Figures S7C and S7D). In parallel, primary TCR-activated CD4$^+$ showed more pronounced dampening of IL-17 release in Th17 vs. Th0 cells (Figure 7D), although NR blunted ROS/RNS (reactive nitrogen species) levels in both lineages (Figure 7E). Furthermore, RNA-seq analysis of CD4$^+$ T cells isolated from subjects consuming placebo and NR showed that NR-responsive DE genes were different between the groups, and PCA plots of the DE genes identified NR supplementation as the PC driving gene expression changes (Figures S7E and S7F; Table S4). Gene set enrichment analysis (GSEA) was performed using the C7 immunologic signature database. Significant GSEA-C7 pathways identified Th1 and Th17 immune cell subsets (Figure 7F). Consistent with this, NR blunted transcript levels of canonical master regulatory transcription factors for Th1 and Th17 polarization, namely, *tbx21* and *rorc*, with no effect on the Th2 regulatory factor *gata3* (Figure 7G). In parallel, activated Th0 cells isolated from subjects taking NR supplementation had significantly higher transcript levels of *sqstm1*, *nqo1*, and *hmox1* and of the genes encoding glutathione biosynthesis, including *gclc* and *gclm* (Figures 7H–7J). Finally, the levels of circulating serum NAM and arginine were elevated in the subjects following *in vivo* NR administration compared with the placebo group (Figure 7K). The differential genes and metabolites identified from the exploratory study were used to construct a network using the Ingenuity Pathway Analysis (IPA) knowledge base. The pathway of oxidative stress genes and arginine biosynthesis regulated by NR was connected to Nrf2 (*NFE2L2*), and the network of gene-metabolite was shown in Figure 7L.

DISCUSSION

This study demonstrated that the immunomodulatory action of NR extends to human CD4$^+$ T cells, where, in an NAD-level-dependent manner, NR blunts both Th1 and Th17 immune responsiveness in healthy volunteers *in vivo* and in healthy control and psoriasis CD4$^+$ T cells *ex vivo*. The dampening of IL-17 appears more robust than that of IFNγ, and in Th0 and Th17 cells, NAD$^+$ boosting appears, via the action of ASL, to increase arginine and fumarate synthesis with subsequent NRF2-mediated transactivation of antioxidant response programs that blunt Th17 polarization and IL-17 production.

The challenge in exploring the mechanisms of action of NAD boosting is its diverse role in metabolic pathways that consume NAD and in the multitude of NAD$^+$-dependent redox enzymes in various cytosolic and mitochondrial metabolic pathways. Furthermore, a question arising is whether different NAD salvage pathway intermediates may have different effects on different extrahepatic tissues.[1] An emerging additional role of NAD may be via the 5′-capping of RNA and a subsequent direct effect on RNA transcription in prokaryotes.[36] The practical ability to answer these questions comprehensively remains technically limited and present, and reductionist approaches are therefore employed to explore this biology. Specifically, a study with an exploratory and validation arm was designed to enable an unbiased and reductionist approach to explore the NR effect on CD4$^+$ T cells. In the exploratory study, NR effects on cells extracted from patients with psoriasis and matched controls *ex vivo* were assessed to identify gene-metabolic networks mediating NR effects. To further assess these findings, the validation study included a double-blinded clinical trial that recruited healthy participants that took either NR or placebo supplements. Using this approach, and by integrating gene-regulatory and metabolic pathway effects, we have identified an anti-inflammatory role of NR supplementation on Th17 immune responsiveness.

Because prior data show that prolonged fasting blunts CD4$^+$ T cell responsiveness,[37] we investigated whether boosting of NAD$^+$, a component of caloric restriction interventions,[38] was sufficient to confer these immunomodulatory effects. To begin to explore whether NAD boosting by NR modulated CD4$^+$ T cell function, we compared healthy volunteers and matched

(K and L) Cellular ROS (K) and mitochondrial ROS (L) in *cd38*- or *sarm1*-KD Th17 cells (n = 4).
(M and N) Protein expression of Nrf2 and Sqstm1 in *cd38*-KD CD4$^+$ T cells (N, n = 8) and *sarm1*-KD cells (N, n = 4–6).
The p values for comparisons of two groups calculated using paired two-tailed Student's t test, or one-way ANOVA when comparing more than two groups (vehicle vs. treated or NC vs. CD38-KD/SARM1-KD). *p < 0.05, **p < 0.01, ***p < 0.001. Histograms represent mean ±SEM.

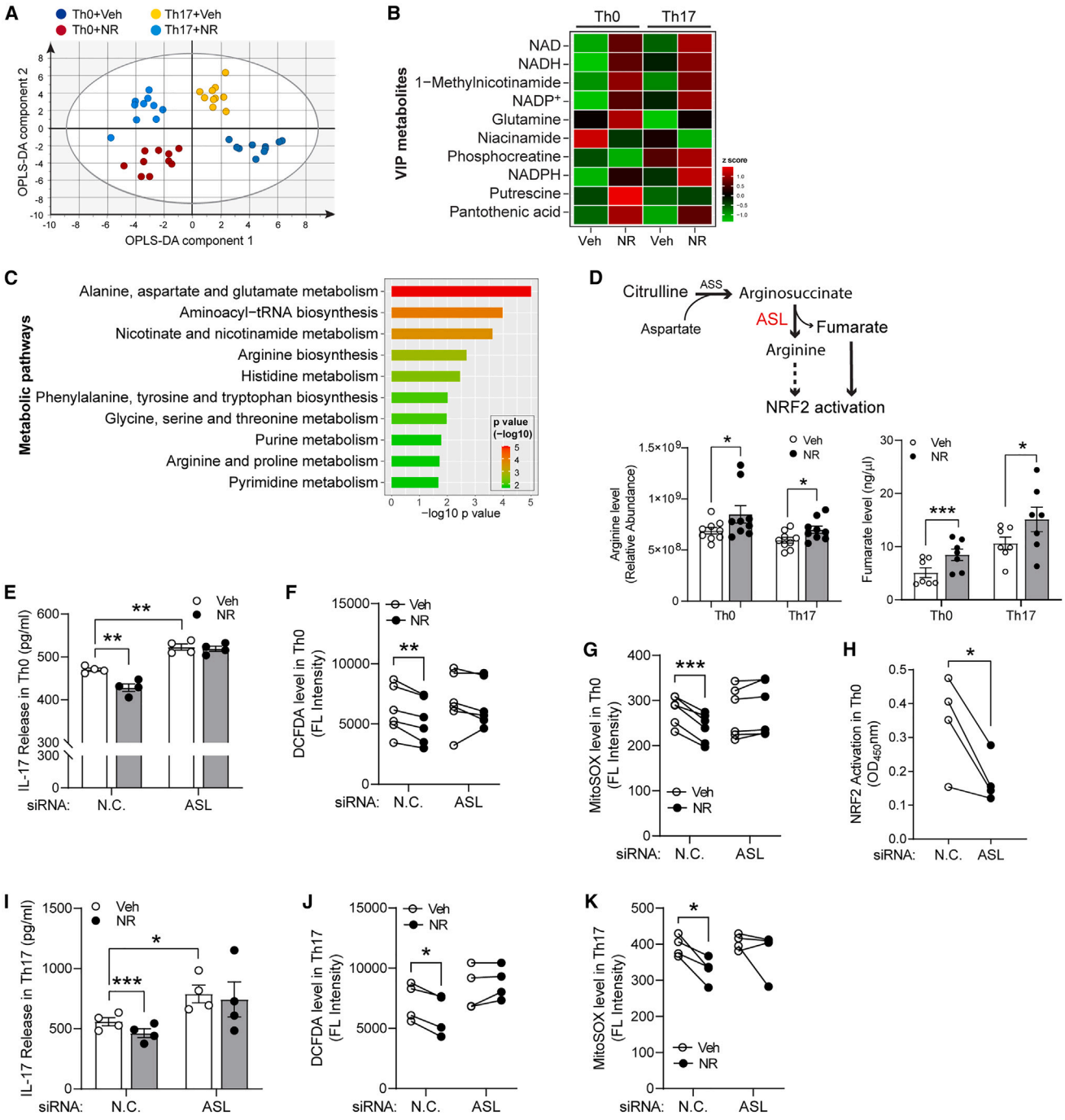

Figure 6. Metabolomics analysis implicates CD4$^+$ T cell fumarate biosynthesis as a mediator of NR's immunomodulatory effect

(A) Orthogonal partial least squares discriminant analysis (OPLS-DA) scatterplot showing separation between vehicle and NR-supplemented sample clusters in Th0 and Th17 differentiated cells, with no significant outliers (n = 10 subjects/group).

(B) The heatmap of relative levels of metabolites with VIP score >1.5 in vehicle control and NR-supplemented groups in Th0 and Th17.

(C) Top 10 pathways enrichment analysis ($p < 0.05$) showing significantly differentiated metabolites (VIP score > 1.0) in vehicle control and NR-supplemented groups in Th0 and Th17 cells.

(D) Metabolic pathway schema showing involvement of arginine pathway metabolites in NRF2 activation. Relative abundance of arginine by light chromatography mass spectrometry (LC/MS) and fumarate assay (Sigma) regulated by NR in Th0 (n = 9) and Th17 (n = 7).

(E) IL-17 release in Th0 following NR after ASL KD for 2 days (n = 4).

(F and G) Cellular ROS (DCFDA, F) and mitochondrial ROS (MitoSOX, G) level after *asl* KD (n = 4–6).

(H) Nrf2 activity in Th0 cells. Active Nrf2 present in the nuclear extract specifically binds to the immobilized NRF2 consensus binding oligonucleotide (n = 4).

(legend continued on next page)

psoriasis patient primary cells *ex vivo*. Initial screening showed that NR had a more robust blunting effect on Th1 and Th17 cytokines rather than on Th2 cytokines, and for the bulk of this study the underlying mechanisms were interrogated while focusing on Th0 and Th17 polarized cells. Because NR has previously been shown to confer robust effects on gene-expression profiles in LPS-activated monocytes,[18] the transcript levels in TCR-activated $CD4^+$ T cells were analyzed and showed substantial regulation in both healthy controls and psoriasis subjects. The initial bioinformatics interrogation of the data focused on the overlapping NR-linked DE genes in control and psoriasis subjects to uncover regulatory programs distinctly responsive to NR. Although numerous pathways were identified, the strongest signal was that NR modulated oxidative stress responses. Subsequent interrogation of validated PPIs based on changes in gene expression uncovered that the Nrf2-Sqstm1-Keap pathway may be operational in this regulation, and the subsequent biochemical and genetic studies supported this conclusion. At the same time a myriad of other pathways were identified that were distinct between the control and psoriasis groups and included changes in RNA metabolism, protein folding and metabolism, intracellular cytoskeletal organization, and signal transduction transcripts. As with the antioxidant control regulatory pathways, these additional regulatory programs will need to be investigated from a reductionist approach to explore their roles in $CD4^+$ T cell immunomodulation. These experiments should also expand our understanding of how NAD^+ boosting controls intracellular $CD4^+$ T cell homeostatic programs.

We next exploited steady-state metabolomics analysis in both Th0 and Th17 $CD4^+$ T cells exposed to NR or placebo to evaluate whether NAD^+-boosting metabolic pathway effects may regulate this biology. As expected, NR increased NAD^+ metabolic intermediates. At the same time, metabolic pathway analysis identified that NAD^+ boosting modified multiple amino acid levels, implicating a role of NR in regulating amino acid metabolism. These metabolic effects probably contribute toward a potential myriad of intracellular immunomodulatory regulatory effects[39] that require exploration. However, in the context of integrating the RNA-seq findings and these metabolic profiles and the established roles of the arginine biosynthetic pathway in immunomodulation,[40] we focused on investigating the effect of the distinct changes in metabolite levels in this pathway. Here arginine and fumarate, both ASL products, are known to activate NRF2 via distinct mechanisms.[29–31] The role of this pathway was confirmed by the abolition of the NR effect by the KD of *asl*. Interestingly, ASL, which breaks down argininosuccinate into arginine with fumarate as a byproduct, is also critical for tyrosine hydroxylase activity, an enzyme linked to catecholamine production.[41] Interestingly, tyrosine hydroxylase activity modulates human T regulatory (Treg) cell function[42] and $CD4^+$ T effector cell polarization.[43,44] Whether NAD^+ boosting modulates Th17 cell polarization and activation via the ASL tyrosine hydroxylase pathway additionally merits further investigation. Finally, although the role of Nrf2 and antioxidant signaling in this immunomodulation is well characterized, additional studies are also required to explore how the additional identified amino acid signaling pathways modulated by NAD boosting collectively contribute to the blunting of Th17 polarization and activation. Furthermore, the effect of increased arginine on nitric oxide biology may play a regulatory role, although metabolites downstream of arginine catabolism were not consistently changed in response to NR.

Reactive oxygen signaling is operational in Th17 differentiation and inflammatory functioning,[45–47] in part via the transcriptional induction of Rorc activity.[45] At the same time, NR has been shown to confer antioxidant effects by augmenting mitochondrial superoxide dismutase activity in monocytes via promoting Sirt3 activation,[17] and NR has been shown to blunt ROS production in PBMCs.[48] In this study, the role of NR in modulating arginine biosynthesis to activate Nrf2 to control ROS levels in $CD4^+$ T cells has been uncovered and shows that NR additionally blunts transcript level of *rorc* after *in vivo* administration. The findings in this study support the prior observation that Nrf2 transactivation blunts Th17 polarization and associated inflammation in the context of murine lupus nephritis.[46]

At the same time, mitochondrial metabolic remodeling is a hallmark of $CD4^+$ T cell activation.[49] Mechanisms uncovered that orchestrate this regulation include mitochondrial metabolism-derived acetyl-CoA in the epigenetic control of inflammatory gene expression[50] and the rate of oxidative phosphorylation itself, which modulates the Th17/Treg cell balance by altering various regulatory control nodes in Th17 differentiation.[51] The RNA-seq data in this study support that NR modulated mitochondrial oxidative metabolism encoding gene expression, and studies show that both redox enzyme control and Sirtuin activation by NAD^+ boosting modulate mitochondrial oxidative phosphorylation. Here, also, further work will be required to explore how these effects of NR specifically attenuate Th17 activation. Also, whether NR modulates Treg differentiation to alter the Th17/Treg balance remains unresolved, although preliminary data of NR from our laboratory did not increase IL-10 secretion in anti-CD3/CD28 activated Th0 cells and *in vivo* NR supplementation did not induce transcript levels encoding IL-10 in PBMCs.[48] Nevertheless, given the role of NAD^+ boosting on mitochondrial biology, cellular metabolism, and ROS biology, the contribution of these metabolic pathways in Treg homeostasis[52] suggests that a more detailed and directed analysis is required to evaluate the direct effect of NAD^+ boosting on Treg biology.

The concept that inflammatory or autoimmune diseases, for example, obesity linked with diabetes and systemic lupus erythematosus,[18,53] are linked to excess NAD^+ consumption because of increased activity of NADase or NAD^+-consuming enzymes is being uncovered.[18,53] In this study, this idea is similarly implicated in psoriasis, given the increased transcript levels of *cd38*, *sarm1*, and *parp* enzymes. These data highlight

(I) IL-17 release in Th17 cells following NR after ASL KD for 2 days (n = 4).

(J and K) Cellular ROS (J) and mitochondrial ROS (K) level after *asl* KD in Th17 cells (n = 4). The p values for comparisons of two groups were calculated using unpaired two-tailed Student's t test (NC vs. *asl*-KD) or paired two-tailed Student's t test (vehicle vs. NR) or by ANOVA for multiple comparisons. All data were represented as mean ± SEM. *p < 0.05, **p < 0.01, ***p < 0.001. Histograms represent mean ±SEM.

CellPress
OPEN ACCESS

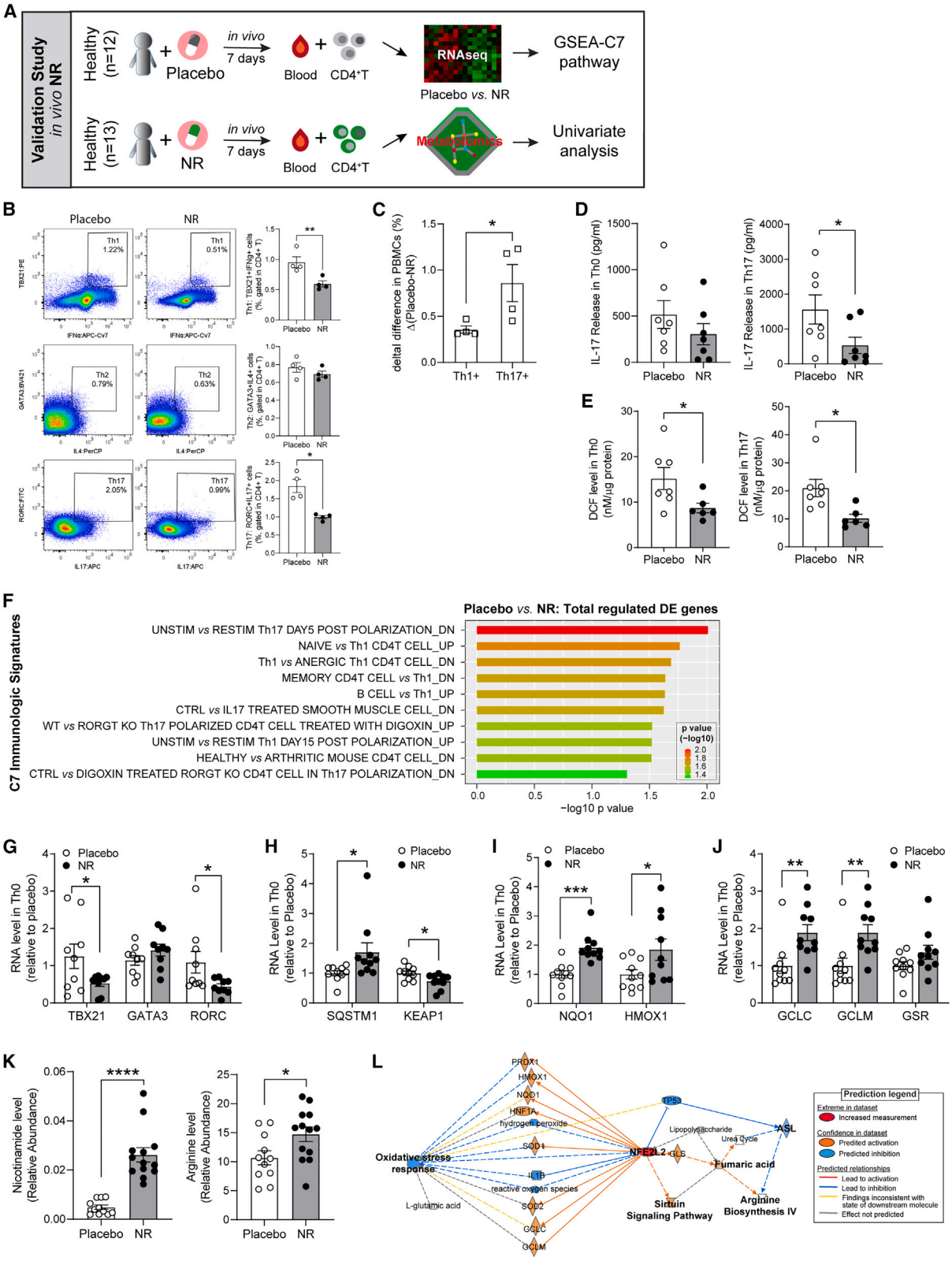

(legend on next page)

the need to further understand the complex interaction of NAD^+ production and consumption pathways and interventions to modulate them in inflammatory and autoimmune diseases. In addition, the finding from this study that NR blunts Th1 and Th17 immune responsiveness in an *ex vivo* study supports that the utilization of NAD^+ boosting could potentially be employed as a supplemental therapy in this disease. The concept is now being explored *in vivo*, where mild-moderate psoriasis patients are being investigated in a placebo-controlled study using the same dose of NR employed for the healthy control population (500 mg BID) as described in this manuscript (ClinicalTrials.gov: NCT04271735).

In conclusion, this study has expanded our understanding of NAD^+ boosting in the adaptive immune system with the focus on NR blunting Th17 immune activity, in part through arginine biosynthesis, Nrf2 activation, and augmentation of cellular antioxidant defense programs. This biology was found to be operational following *ex vivo* supplementation in healthy control subjects, in psoriasis subjects, and in healthy volunteers following oral supplementation. The systems biological approaches employed in this study uncover numerous additional metabolic and gene-regulatory pathways to explore whereby NAD^+ boosting modulates immunometabolism and immune regulation. Furthermore, this study advances our understanding of the role of NAD^+ boosting in immunoregulation and lays the foundation for future studies in humans with inflammatory diseases, including psoriasis.

Limitations of the study

Although this study shows a clear role of NR supplementation in blunting Th17 activity, as discussed, multiple potential levels of regulation remain to be uncovered. In addition, NR appears to have a similar, albeit more modest, effect in blunting Th1 differentiation and activation, and this biology has not been explored. It should also be noted that despite inflammatory cell dampening effects of NAD^+ boosting, murine and clinical studies suggest that these metabolic interventions may concurrently augment cytotoxic TIL function[8,9] and blunt cancer risk.[54] Nevertheless, larger and longer-term studies will need to be performed to evaluate the putative cancer risk in the context of inflammatory or autoimmune diseases.

STAR★METHODS

Detailed methods are provided in the online version of this paper and include the following:

- KEY RESOURCES TABLE
- RESOURCE AVAILABILITY
  - Lead contact
  - Materials availability
  - Data and code availability
- EXPERIMENTAL MODEL AND SUBJECT DETAILS
  - Study design and human subjects
  - Clinical protocol of placebo/NR study
- METHOD DETAILS
  - Flow cytometry immunophenotyping
  - Human $CD4^+$ T cell Isolation and cytokine assay
  - RNA sequencing and bioinformatics analysis
  - Inhibitors, siRNAs, and lentiviruses
  - RNA Isolation and Quantitative PCR analysis
  - Western Blotting
  - Intracellular ROS and mitochondrial ROS assay
  - NRF2 activation assay
  - Fumarate assay
  - Metabolomics and Data Analysis
  - Statistical analysis
- ADDITIONAL RESOURCES

SUPPLEMENTAL INFORMATION

Supplemental information can be found online at https://doi.org/10.1016/j.xcrm.2023.101157.

ACKNOWLEDGMENTS

We thank Myron Waclawiw of the NHLBI Biostatistics Branch for assistance with the clinical protocol design, Chromadex for supplying NR and matching placebo capsules for the *in vivo* study and NR powder for the cell culture

Figure 7. *In vivo* supplementation of NR in healthy volunteers recapitulated the NR regulatory effects on $CD4^+$ T cell activation

(A) Schema describing the validation study to assess whether NR mirrors this immunomodulation *in vivo*. This was a double-blinded study of healthy participants consuming NR or placebo. Subsequent metabolomics and gene-expression profiling datasets were employed to evaluate pathways identified in the exploratory study (Figure 1E).

(B) Representative flow cytometry of PBMCs from placebo- and NR-administrated subjects for 7 days. The dot-line plots show cell population (percentiles) gated to $CD4^+$ cells. Th1, $Tbx21^+IFN\gamma^+$; Th2, $Gata3^+IL4^+$; Th17, $Rorc^+IL17^+$ (n = 4/group).

(C) Differential Th1 and Th17 levels in response to NR compared with placebo (n = 4).

(D) IL-17 cytokine release in $CD4^+$ Th0- and Th17-differentiated cells from placebo- and NR-administrated subjects. $CD4^+$ T cells were isolated in the refed state, differentiated into Th17 cells, and exposed to TCR activation (placebo, n = 7; NR, n = 7). Unpaired two-tailed Student's t test.

(E) ROS/RNS (reactive nitrogen species) activity measured in Th0 and Th17 lysates by OxiSelect ROS/RNS Assay (placebo, n = 7; NR, n = 6).

(F) GSEA-C7 pathway analysis of DE genes (2,380) from placebo vs. NR of naive $CD4^+$ T cells (placebo, n = 8; NR, n = 7).

(G) RNA expression T cell regulatory transcriptional factors (*tbx21* for Th1, *gata3* for Th2, *rorc* for Th17) in activated Th0 cells from placebo and NR groups (n = 9/group). Data were normalized to ef1α and represented as mean ± SEM.

(H–J) RNA expression level of *sqstm1*, *keap1* (H), ROS detoxification-related genes (I, *nqo1* and *hmox1*), and glutathione synthesis-related genes (J, *gclc, gclm*, and *gsr*) in activated Th0 cells from both groups (n = 9/group). Data were normalized to 18S rRNA and represented as mean ± SEM.

(K) Relative abundance of nicotinamide and arginine by LC/MS in serum from placebo (n = 11) and NR (n = 13) groups. Unpaired two-tailed (placebo vs. NR) Student's t test. *$p < 0.05$, **$p < 0.01$, ***$p < 0.001$.

(L) The differential genes and metabolites identified from the exploratory study arm were employed to construct a network by Ingenuity Pathway Analysis (IPA). Each colored node in the network is a gene/metabolite regulated by NR. The connection between the indicated nodes utilizes IPA network information to predict activation or inhibitory relationships. The biological process or groups of molecules are represented as white nodes. Histograms represent mean ±SEM.

studies, and an NIH Bench-to-Bedside award for supplemental funding. We additionally thank Dr. Nina Klimova, formerly of the NHLBI, and Dr. Yun-Wei A. Hsu for their support of the metabolomics analysis at the Northwest Metabolomics Research Center of the University of Washington (NIH grant 1S10OD021562-01). We thank and acknowledge the assistance of the NHLBI DNA Sequencing and Genomics Core in performing the RNA library sequencing and Dr. Pradeep Dagur in the NHLBI Flow Cytometry Core for performing the immunophenotyping. Trial registration was as follows: ClinicalTrials.gov: NCT01934660, NCT02812238, and NCT01143454 and NIH Clinical Center blood bank (ClinicalTrials.gov: NCT00001846). This work was supported by the NHLBI Division of Intramural Research (ZIA-HL005102 to M.N.S.), NIH Bench-to-Bedside award (HL-129510-04S1 to M.N.S. and R.T.) and the NIH Office of Dietary Supplements (J.T.), the Spanish Ministry of Science and Innovation (RYC2018-026050-I and PID2019-105665RA-I00 to J.T.), and the UK MRC (MR/P011705/2 and UKDRI-5002 to J.L.G.; MAP UK).

AUTHOR CONTRIBUTIONS

Conceived the project, K.H., K.S., S.H., J.W., and M.N.S.; secured funding, M.N.S. and J.T.; designed the experiments, K.H., K.S., J.W., R.D.H., H.L.T., N.N.M., J.T., and M.N.S.; recruited study subjects, R.D.H., H.L.T., and N.N.M.; carried out experiments, K.H., K.S., R.S., S.H., H.G.-H., J.W., R.T., and J.T.; analyzed data, K.H., K.S., A.M.M., R.S., H.G.-H., R.T., J.T., and M.N.S.; wrote the manuscript, K.H., K.S., and M.N.S.; edited the manuscript, A.M.M., H.L.T., N.N.M., and J.T.

DECLARATION OF INTERESTS

The NR and matching placebo were supplied by Chromadex Inc. (Los Angeles, CA, USA) under a Cooperative and Development Research Agreement (CRADA).

INCLUSION AND DIVERSITY

We support inclusive, diverse, and equitable conduct of research.

Received: December 1, 2022
Revised: May 23, 2023
Accepted: July 18, 2023
Published: August 15, 2023

REFERENCES

1. Chini, C.C.S., Zeidler, J.D., Kashyap, S., Warner, G., and Chini, E.N. (2021). Evolving concepts in NAD(+) metabolism. Cell Metab. *33*, 1076–1087. https://doi.org/10.1016/j.cmet.2021.04.003.
2. Massudi, H., Grant, R., Braidy, N., Guest, J., Farnsworth, B., and Guillemin, G.J. (2012). Age-associated changes in oxidative stress and NAD+ metabolism in human tissue. PLoS One *7*, e42357. https://doi.org/10.1371/journal.pone.0042357.
3. de Guia, R.M., Agerholm, M., Nielsen, T.S., Consitt, L.A., Søgaard, D., Helge, J.W., Larsen, S., Brandauer, J., Houmard, J.A., and Treebak, J.T. (2019). Aerobic and resistance exercise training reverses age-dependent decline in NAD(+) salvage capacity in human skeletal muscle. Physiol. Rep. *7*, e14139. https://doi.org/10.14814/phy2.14139.
4. Yoshino, J., Mills, K.F., Yoon, M.J., and Imai, S.I. (2011). Nicotinamide mononucleotide, a key NAD(+) intermediate, treats the pathophysiology of diet- and age-induced diabetes in mice. Cell Metab. *14*, 528–536. https://doi.org/10.1016/j.cmet.2011.08.014.
5. Abdellatif, M., Trummer-Herbst, V., Koser, F., Durand, S., Adão, R., Vasques-Nóvoa, F., Freundt, J.K., Voglhuber, J., Pricolo, M.R., Kasa, M., et al. (2021). Nicotinamide for the treatment of heart failure with preserved ejection fraction. Sci. Transl. Med. *13*, eabd7064. https://doi.org/10.1126/scitranslmed.abd7064.
6. Katsuyama, E., Suarez-Fueyo, A., Bradley, S.J., Mizui, M., Marin, A.V., Mulki, L., Krishfield, S., Malavasi, F., Yoon, J., Sui, S.J.H., et al. (2020). The CD38/NAD/SIRTUIN1/EZH2 Axis Mitigates Cytotoxic CD8 T Cell Function and Identifies Patients with SLE Prone to Infections. Cell Rep. *30*, 112–123.e4. https://doi.org/10.1016/j.celrep.2019.12.014.
7. Navas, L.E., and Carnero, A. (2021). NAD(+) metabolism, stemness, the immune response, and cancer. Signal Transduct. Target. Ther. *6*, 2. https://doi.org/10.1038/s41392-020-00354-w.
8. Wang, Y., Wang, F., Wang, L., Qiu, S., Yao, Y., Yan, C., Xiong, X., Chen, X., Ji, Q., Cao, J., et al. (2021). NAD(+) supplement potentiates tumor-killing function by rescuing defective TUB-mediated NAMPT transcription in tumor-infiltrated T cells. Cell Rep. *36*, 109516. https://doi.org/10.1016/j.celrep.2021.109516.
9. Yu, Y.R., Imrichova, H., Wang, H., Chao, T., Xiao, Z., Gao, M., Rincon-Restrepo, M., Franco, F., Genolet, R., Cheng, W.C., et al. (2020). Disturbed mitochondrial dynamics in CD8(+) TILs reinforce T cell exhaustion. Nat. Immunol. *21*, 1540–1551. https://doi.org/10.1038/s41590-020-0793-3.
10. Kaneko, S., Wang, J., Kaneko, M., Yiu, G., Hurrell, J.M., Chitnis, T., Khoury, S.J., and He, Z. (2006). Protecting axonal degeneration by increasing nicotinamide adenine dinucleotide levels in experimental autoimmune encephalomyelitis models. J. Neurosci. *26*, 9794–9804. https://doi.org/10.1523/JNEUROSCI.2116-06.2006.
11. Baixauli, F., Acín-Pérez, R., Villarroya-Beltrí, C., Mazzeo, C., Nuñez-Andrade, N., Gabandé-Rodriguez, E., Ledesma, M.D., Blázquez, A., Martin, M.A., Falcón-Pérez, J.M., et al. (2015). Mitochondrial Respiration Controls Lysosomal Function during Inflammatory T Cell Responses. Cell Metab. *22*, 485–498. https://doi.org/10.1016/j.cmet.2015.07.020.
12. Trammell, S.A.J., Weidemann, B.J., Chadda, A., Yorek, M.S., Holmes, A., Coppey, L.J., Obrosov, A., Kardon, R.H., Yorek, M.A., and Brenner, C. (2016). Nicotinamide Riboside Opposes Type 2 Diabetes and Neuropathy in Mice. Sci. Rep. *6*, 26933. https://doi.org/10.1038/srep26933.
13. Navarro, M.N., Gómez de las Heras, M.M., and Mittelbrunn, M. (2021). Nicotinamide adenine dinucleotide metabolism in the immune response, autoimmunity and inflammageing. Br. J. Pharmacol. *179*, 1839–1856. https://doi.org/10.1111/bph.15477.
14. Mills, K.F., Yoshida, S., Stein, L.R., Grozio, A., Kubota, S., Sasaki, Y., Redpath, P., Migaud, M.E., Apte, R.S., Uchida, K., et al. (2016). Long-Term Administration of Nicotinamide Mononucleotide Mitigates Age-Associated Physiological Decline in Mice. Cell Metab. *24*, 795–806. https://doi.org/10.1016/j.cmet.2016.09.013.
15. Hou, Y., Lautrup, S., Cordonnier, S., Wang, Y., Croteau, D.L., Zavala, E., Zhang, Y., Moritoh, K., O'Connell, J.F., Baptiste, B.A., et al. (2018). NAD(+) supplementation normalizes key Alzheimer's features and DNA damage responses in a new AD mouse model with introduced DNA repair deficiency. Proc. Natl. Acad. Sci. USA *115*, E1876-E1885. https://doi.org/10.1073/pnas.1718819115.
16. Elhassan, Y.S., Kluckova, K., Fletcher, R.S., Schmidt, M.S., Garten, A., Doig, C.L., Cartwright, D.M., Oakey, L., Burley, C.V., Jenkinson, N., et al. (2019). Nicotinamide Riboside Augments the Aged Human Skeletal Muscle NAD(+) Metabolome and Induces Transcriptomic and Anti-inflammatory Signatures. Cell Rep. *28*, 1717–1728.e6. https://doi.org/10.1016/j.celrep.2019.07.043.
17. Traba, J., Kwarteng-Siaw, M., Okoli, T.C., Li, J., Huffstutler, R.D., Bray, A., Waclawiw, M.A., Han, K., Pelletier, M., Sauve, A.A., et al. (2015). Fasting and refeeding differentially regulate NLRP3 inflammasome activation in human subjects. J. Clin. Invest. *125*, 4592–4600. https://doi.org/10.1172/JCI83260.
18. Wu, J., Singh, K., Lin, A., Meadows, A.M., Wu, K., Shing, V., Bley, M., Hassanzadeh, S., Huffstutler, R.D., Schmidt, M.S., et al. (2022). Boosting NAD+ blunts TLR4-induced type I IFN in control and systemic lupus erythematosus monocytes. J. Clin. Invest. *132*, e139828. https://doi.org/10.1172/JCI139828.
19. Zhou, B., Wang, D.D.H., Qiu, Y., Airhart, S., Liu, Y., Stempien-Otero, A., O'Brien, K.D., and Tian, R. (2020). Boosting NAD level suppresses inflammatory activation of PBMCs in heart failure. J. Clin. Invest. *130*, 6054–6063. https://doi.org/10.1172/JCI138538.

20. Brakedal, B., Dölle, C., Riemer, F., Ma, Y., Nido, G.S., Skeie, G.O., Craven, A.R., Schwarzlmüller, T., Brekke, N., Diab, J., et al. (2022). The NADPARK study: A randomized phase I trial of nicotinamide riboside supplementation in Parkinson's disease. Cell Metab. *34*, 396–407.e6. https://doi.org/10.1016/j.cmet.2022.02.001.

21. Heer, C.D., Sanderson, D.J., Voth, L.S., Alhammad, Y.M.O., Schmidt, M.S., Trammell, S.A.J., Perlman, S., Cohen, M.S., Fehr, A.R., and Brenner, C. (2020). Coronavirus infection and PARP expression dysregulate the NAD metabolome: An actionable component of innate immunity. J. Biol. Chem. *295*, 17986–17996. https://doi.org/10.1074/jbc.RA120.015138.

22. Lerman, J.B., Joshi, A.A., Chaturvedi, A., Aberra, T.M., Dey, A.K., Rodante, J.A., Salahuddin, T., Chung, J.H., Rana, A., Teague, H.L., et al. (2017). Coronary Plaque Characterization in Psoriasis Reveals High-Risk Features That Improve After Treatment in a Prospective Observational Study. Circulation *136*, 263–276. https://doi.org/10.1161/CIRCULATIONAHA.116.026859.

23. Dey, A.K., Joshi, A.A., Chaturvedi, A., Lerman, J.B., Aberra, T.M., Rodante, J.A., Teague, H.L., Harrington, C.L., Rivers, J.P., Chung, J.H., et al. (2017). Association Between Skin and Aortic Vascular Inflammation in Patients With Psoriasis: A Case-Cohort Study Using Positron Emission Tomography/Computed Tomography. JAMA Cardiol. *2*, 1013–1018. https://doi.org/10.1001/jamacardio.2017.1213.

24. Abdallah, M.A., Abdel-Hamid, M.F., Kotb, A.M., and Mabrouk, E.A. (2009). Serum interferon-gamma is a psoriasis severity and prognostic marker. Cutis *84*, 163–168.

25. Brembilla, N.C., Senra, L., and Boehncke, W.H. (2018). The IL-17 Family of Cytokines in Psoriasis: IL-17A and Beyond. Front. Immunol. *9*, 1682. https://doi.org/10.3389/fimmu.2018.01682.

26. Leonardi, C.L., Powers, J.L., Matheson, R.T., Goffe, B.S., Zitnik, R., Wang, A., and Gottlieb, A.B.; Etanercept Psoriasis Study Group (2003). Etanercept as monotherapy in patients with psoriasis. N. Engl. J. Med. *349*, 2014–2022. https://doi.org/10.1056/NEJMoa030409.

27. Leonardi, C., Matheson, R., Zachariae, C., Cameron, G., Li, L., Edson-Heredia, E., Braun, D., and Banerjee, S. (2012). Anti-interleukin-17 monoclonal antibody ixekizumab in chronic plaque psoriasis. N. Engl. J. Med. *366*, 1190–1199. https://doi.org/10.1056/NEJMoa1109997.

28. Mease, P.J. (2015). Inhibition of interleukin-17, interleukin-23 and the TH17 cell pathway in the treatment of psoriatic arthritis and psoriasis. Curr. Opin. Rheumatol. *27*, 127–133. https://doi.org/10.1097/BOR.0000000000000147.

29. Zhao, Y., Jiang, Q., Zhang, X., Zhu, X., Dong, X., Shen, L., Zhang, S., Niu, L., Chen, L., Zhang, M., et al. (2021). l-Arginine Alleviates LPS-Induced Oxidative Stress and Apoptosis via Activating SIRT1-AKT-Nrf2 and SIRT1-FOXO3a Signaling Pathways in C2C12 Myotube Cells. Antioxidants *10*, 1957. https://doi.org/10.3390/antiox10121957.

30. Burgener, A.V., Bantug, G.R., Meyer, B.J., Higgins, R., Ghosh, A., Bignucolo, O., Ma, E.H., Loeliger, J., Unterstab, G., Geigges, M., et al. (2019). SDHA gain-of-function engages inflammatory mitochondrial retrograde signaling via KEAP1-Nrf2. Nat. Immunol. *20*, 1311–1321. https://doi.org/10.1038/s41590-019-0482-2.

31. Liang, M., Wang, Z., Li, H., Cai, L., Pan, J., He, H., Wu, Q., Tang, Y., Ma, J., and Yang, L. (2018). l-Arginine induces antioxidant response to prevent oxidative stress via stimulation of glutathione synthesis and activation of Nrf2 pathway. Food Chem. Toxicol. *115*, 315–328. https://doi.org/10.1016/j.fct.2018.03.029.

32. Katsuragi, Y., Ichimura, Y., and Komatsu, M. (2015). p62/SQSTM1 functions as a signaling hub and an autophagy adaptor. FEBS J. *282*, 4672–4678. https://doi.org/10.1111/febs.13540.

33. Jain, A., Lamark, T., Sjøttem, E., Larsen, K.B., Awuh, J.A., Øvervatn, A., McMahon, M., Hayes, J.D., and Johansen, T. (2010). p62/SQSTM1 is a target gene for transcription factor NRF2 and creates a positive feedback loop by inducing antioxidant response element-driven gene transcription. J. Biol. Chem. *285*, 22576–22591. https://doi.org/10.1074/jbc.M110.118976.

34. Ma, Y., Wu, D., Ding, X., and Ying, W. (2014). CD38 plays key roles in both antioxidation and cell survival of H2O2-treated primary rodent astrocytes. Int. J. Physiol. Pathophysiol. Pharmacol. *6*, 102–108.

35. Hughes, R.O., Bosanac, T., Mao, X., Engber, T.M., DiAntonio, A., Milbrandt, J., Devraj, R., and Krauss, R. (2021). Small Molecule SARM1 Inhibitors Recapitulate the SARM1(-/-) Phenotype and Allow Recovery of a Metastable Pool of Axons Fated to Degenerate. Cell Rep. *34*, 108588. https://doi.org/10.1016/j.celrep.2020.108588.

36. Julius, C., and Yuzenkova, Y. (2019). Noncanonical RNA-capping: Discovery, mechanism, and physiological role debate. Wiley Interdiscip. Rev. RNA *10*, e1512. https://doi.org/10.1002/wrna.1512.

37. Han, K., Singh, K., Rodman, M.J., Hassanzadeh, S., Wu, K., Nguyen, A., Huffstutler, R.D., Seifuddin, F., Dagur, P.K., Saxena, A., et al. (2021). Fasting-induced FOXO4 blunts human CD4(+) T helper cell responsiveness. Nat. Metab. *3*, 318–326. https://doi.org/10.1038/s42255-021-00356-0.

38. Belenky, P., Bogan, K.L., and Brenner, C. (2007). NAD+ metabolism in health and disease. Trends Biochem. Sci. *32*, 12–19. https://doi.org/10.1016/j.tibs.2006.11.006.

39. Proietti, E., Rossini, S., Grohmann, U., and Mondanelli, G. (2020). Polyamines and Kynurenines at the Intersection of Immune Modulation. Trends Immunol. *41*, 1037–1050. https://doi.org/10.1016/j.it.2020.09.007.

40. Wijnands, K.A.P., Castermans, T.M.R., Hommen, M.P.J., Meesters, D.M., and Poeze, M. (2015). Arginine and citrulline and the immune response in sepsis. Nutrients *7*, 1426–1463. https://doi.org/10.3390/nu7031426.

41. Lerner, S., Anderzhanova, E., Verbitsky, S., Eilam, R., Kuperman, Y., Tsoory, M., Kuznetsov, Y., Brandis, A., Mehlman, T., Mazkereth, R., et al. (2019). ASL Metabolically Regulates Tyrosine Hydroxylase in the Nucleus Locus Coeruleus. Cell Rep. *29*, 2144–2153.e7. https://doi.org/10.1016/j.celrep.2019.10.043.

42. Cosentino, M., Fietta, A.M., Ferrari, M., Rasini, E., Bombelli, R., Carcano, E., Saporiti, F., Meloni, F., Marino, F., and Lecchini, S. (2007). Human CD4+CD25+ regulatory T cells selectively express tyrosine hydroxylase and contain endogenous catecholamines subserving an autocrine/paracrine inhibitory functional loop. Blood *109*, 632–642. https://doi.org/10.1182/blood-2006-01-028423.

43. Zhao, X.Y., Cui, S.W., Wang, X.Q., Peng, Y.P., and Qiu, Y.H. (2013). Tyrosine hydroxylase expression in CD4(+) T cells is associated with joint inflammatory alleviation in collagen type II-induced arthritis. Rheumatol. Int. *33*, 2597–2605. https://doi.org/10.1007/s00296-013-2788-y.

44. Liu, Y., Huang, Y., Wang, X.Q., Peng, Y.P., and Qiu, Y.H. (2012). Effect of tyrosine hydroxylase gene silencing in CD4+ T lymphocytes on differentiation and function of helper T cells. Neuroendocrinol. Lett. *33*, 643–650.

45. Zhi, L., Ustyugova, I.V., Chen, X., Zhang, Q., and Wu, M.X. (2012). Enhanced Th17 differentiation and aggravated arthritis in IEX-1-deficient mice by mitochondrial reactive oxygen species-mediated signaling. J. Immunol. *189*, 1639–1647. https://doi.org/10.4049/jimmunol.1200528.

46. Zhao, M., Chen, H., Ding, Q., Xu, X., Yu, B., and Huang, Z. (2016). Nuclear Factor Erythroid 2-related Factor 2 Deficiency Exacerbates Lupus Nephritis in B6/lpr mice by Regulating Th17 Cell Function. Sci. Rep. *6*, 38619. https://doi.org/10.1038/srep38619.

47. Kaufmann, U., Kahlfuss, S., Yang, J., Ivanova, E., Koralov, S.B., and Feske, S. (2019). Calcium Signaling Controls Pathogenic Th17 Cell-Mediated Inflammation by Regulating Mitochondrial Function. Cell Metab. *29*, 1104–1118.e6. https://doi.org/10.1016/j.cmet.2019.01.019.

48. Wang, D.D., Airhart, S.E., Zhou, B., Shireman, L.M., Jiang, S., Melendez Rodriguez, C., Kirkpatrick, J.N., Shen, D.D., Tian, R., and O'Brien, K.D. (2022). Safety and Tolerability of Nicotinamide Riboside in Heart Failure With Reduced Ejection Fraction. JACC. Basic Transl. Sci. *7*, 1183–1196. https://doi.org/10.1016/j.jacbts.2022.06.012.

49. Sack, M.N. (2018). Mitochondrial fidelity and metabolic agility control immune cell fate and function. J. Clin. Invest. *128*, 3651–3661. https://doi.org/10.1172/JCI120845.

50. Hochrein, S.M., Wu, H., Eckstein, M., Arrigoni, L., Herman, J.S., Schumacher, F., Gerecke, C., Rosenfeldt, M., Grün, D., Kleuser, B., et al. (2022). The glucose transporter GLUT3 controls T helper 17 cell responses through glycolytic-epigenetic reprogramming. Cell Metab. *34*, 516–532.e11. https://doi.org/10.1016/j.cmet.2022.02.015.

51. Shin, B., Benavides, G.A., Geng, J., Koralov, S.B., Hu, H., Darley-Usmar, V.M., and Harrington, L.E. (2020). Mitochondrial Oxidative Phosphorylation Regulates the Fate Decision between Pathogenic Th17 and Regulatory T Cells. Cell Rep. *30*, 1898–1909.e4. https://doi.org/10.1016/j.celrep.2020.01.022.

52. Steinert, E.M., Vasan, K., and Chandel, N.S. (2021). Mitochondrial Metabolism Regulation of T Cell-Mediated Immunity. Annu. Rev. Immunol. *39*, 395–416. https://doi.org/10.1146/annurev-immunol-101819-082015.

53. van Beek, L., Lips, M.A., Visser, A., Pijl, H., Ioan-Facsinay, A., Toes, R., Berends, F.J., Willems van Dijk, K., Koning, F., and van Harmelen, V. (2014). Increased systemic and adipose tissue inflammation differentiates obese women with T2DM from obese women with normal glucose tolerance. Metabolism *63*, 492–501. https://doi.org/10.1016/j.metabol.2013.12.002.

54. Chen, A.C., Martin, A.J., Choy, B., Fernández-Peñas, P., Dalziell, R.A., McKenzie, C.A., Scolyer, R.A., Dhillon, H.M., Vardy, J.L., Kricker, A., et al. (2015). A Phase 3 Randomized Trial of Nicotinamide for Skin-Cancer Chemoprevention. N. Engl. J. Med. *373*, 1618–1626. https://doi.org/10.1056/NEJMoa1506197.

55. Jensen, L.J., Kuhn, M., Stark, M., Chaffron, S., Creevey, C., Muller, J., Doerks, T., Julien, P., Roth, A., Simonovic, M., et al. (2009). STRING 8--a global view on proteins and their functional interactions in 630 organisms. Nucleic Acids Res. *37*, D412-D416. https://doi.org/10.1093/nar/gkn760.

56. Yu, G., Wang, L.G., Han, Y., and He, Q.Y. (2012). clusterProfiler: an R package for comparing biological themes among gene clusters. OMICS *16*, 284–287. https://doi.org/10.1089/omi.2011.0118.

57. Shannon, P., Markiel, A., Ozier, O., Baliga, N.S., Wang, J.T., Ramage, D., Amin, N., Schwikowski, B., and Ideker, T. (2003). Cytoscape: a software environment for integrated models of biomolecular interaction networks. Genome Res. *13*, 2498–2504. https://doi.org/10.1101/gr.1239303.

STAR★METHODS

KEY RESOURCES TABLE

REAGENT or RESOURCE	SOURCE	IDENTIFIER
Antibodies		
Rabbit monoclonal anti-NRF2 (E3J1V)	Cell Signaling	Cat# 33649; RRID: N/A
Rabbit monoclonal anti-SQSTM1/p62 (D1Q5S)	Cell Signaling	Cat# 39749; RRID: AB_2799160
Rabbit monoclonal anti-KEAP1 (D6B12)	Cell Signaling	Cat# 8047; RRID: AB_10860776
Rabbit monoclonal anti-NQO1 (D6H3A)	Cell Signaling	Cat# 62262; RRID: AB_2799623
Rabbit polyclonal anti-CD38	Cell Signaling	Cat# 92457; RRID: N/A
Rabbit monoclonal anti-SARM1 (D2M5I)	Cell Signaling	Cat# 13022; RRID: AB_2798090
Mouse monoclonal anti-ACTIN (C4)	Millipore	Cat. MAB1501; RRID: AB_2223041
IRDye800CW Goat anti-rabbit IgG	Li-Cor Bioscience	Cat. 926-32211; PRID: AB_621843
IRDye680RD Donkey anti-mouse IgG	Li-Cor Bioscience	Cat. 926-68072; RRID: AB_10954628
IRDye680RD Goat anti-rabbit IgG	Li-Cor Bioscience	Cat. 926-68071; RRID: AB_10956166
Mouse monoclonal anti-human CD3	Biolegend	Cat. 317326; RRID: AB_11150592
Mouse monoclonal anti-human CD28	Biolegend	Cat. 302934; RRID: AB_11148949
Mouse monoclonal anti-human IFNγ	eBioscience	Cat. 16731885; RRID: AB_469251
Mouse monoclonal anti-human IL-4	eBioscience	Cat. 16704885; RRID: AB_469211
Flow cytometry immunophenotyping		This paper; See Table S5 for details
Bacterial and virus strains		
One Shot TOP10*E. coli*	ThermoFisher Scientific	Cat. C404003
pLenti-c-Myc-DDK	Origene Technologies	Cat. PS100064
pLenti-c-Myc-DDK-NRF2	Origene Technologies	Cat. RC204140L2
pLenti-c-Myc-DDK-SQSTM1	Origene Technologies	Cat. RC203214L1
Biological samples		
Human serum	From subject cohort -	NIH Clinical Center Blood Bank ClinicalTrials.gov ID-NCT01143454/ NCT01934660/NCT02812238
Chemicals, peptides, and recombinant proteins		
Nicotinamide Riboside	ChromaDex	Cat. ASB-00014315-005
L-Arginine	Sigma	Cat. A5006
Rucaparib camsylate	Sigma	Cat. PZ0036
Compound 78c	Selleckchem	Cat. S8960
ML385	Selleckchem	Cat. S8790
DMF	Selleckchem	Cat. S2586
DCFDA (2',7'-Dichlorofluorescin Diacetate)	Sigma	Cat. 287810
MitoSOX red	Invitrogen	Cat. M36008
DEAE-Dextran	Sigma	Cat. D9885
LIVE/DEAD Fixable Yellow Dead Cell Stain Kit	Invitrogen	Cat. L34959
PMA	Sigma	Cat. P8139
Cell stimulation cocktail plus protein transport inhibitors	eBioscience	Cat. 00-4975-93
FoxP3 Transcription Factor Staining Buffer Set	eBioscience	Cat. 00-5523-00
Human IL-4 Recombinant protein	Peprotech	Cat. 200-04B
Human IL-6 Recombinant protein	Peprotech	Cat. 200-06B
Human IL-12 Recombinant protein	Peprotech	Cat. 200-12B
Human IL-23 Recombinant protein	Peprotech	Cat. 200-23B
Human TGF-β1 Recombinant protein	Peprotech	Cat. 100-21B
Human IL-1β Recombinant protein	Peprotech	Cat. 200-01B

(*Continued on next page*)

Continued

REAGENT or RESOURCE	SOURCE	IDENTIFIER
Critical commercial assays		
CyQuant Cell Proliferation Assay	Invitrogen	Cat. C7026
Pierce BCA Protein Assay	Thermo Scientific	Cat. 23227
Lipid Peroxidation (4-HNE) Assay Kit	Abcam	Cat. ab238538
OxiSelect *in vitro* ROS/RNS assay kit	Cell Biolabs	Cat. STA-347
Antioxidant assay kit	Sigma	Cat. CS0790
GSH/GSSG ratio detection assay	Abcam BioVision	Cat. ab138881 Cat. K264
GSH assay kit	BioAssay Systems	Cat. DIGT-250
NRF2 Transcription Factor Assay Kit	Abcam	Cat. ab207223
Nuclear extraction kit	Abcam	Cat. ab113474
Fumarate Assay Kit	Sigma	Cat. MAK060
Human IFNγ Duoset ELISA Kit	R&D Systems	Cat. DY285B
Human IL-4 Duoset ELISA Kit	R&D Systems	Cat. DY204
Human IL-5 Duoset ELISA Kit	R&D Systems	Cat. DY205
Human IL-17 Duoset ELISA Kit	R&D Systems	Cat. DY317
Deposited data		
RNAseq data	This paper; See Tables S1, S2, and S4 for details	GEO database: GSE237556
Metabolomics data	This paper; See Table S3 for details	Mendeley database: https://data.mendeley.com/datasets/hskhyyss4c/1
Experimental models: Cell lines		
HEK293T		N/A
Experimental models: Organisms/strains		
Human subjects	NIH	NIH Clinical Center Blood Bank ClinicalTrials.gov ID-NCT01143454/ NCT01934660/NCT02812238
Oligonucleotides		
Primers for RT-PCR	This paper; See Table S7 for details	N/A
Accell Non-targeting Control	Dharmacon	Cat. D-001910-01-20
SMARTpool: Accell NFE2L2	Dharmacon	Cat. E-003755-00-0010
SMARTpool: Accell SQTM1	Dharmacon	Cat. E-010230-00-0010
SMARTpool: Accell GCLC	Dharmacon	Cat. E-009212-00-0010
SMARTpool: Accell GCLM	Dharmacon	Cat. E-011670-00-0010
SMARTpool: Accell GSR	Dharmacon	Cat. E-009647-00-0010
SMARTpool: Accell ASL	Dharmacon	Cat. E-008840-00-0020
SMARTpool: Accell CD38	Dharmacon	Cat. E-009222-00-0010
SMARTpool: Accell SARM1	Dharmacon	Cat. E-008076-00-0010
Recombinant DNA		
psPAX2	Addgene	Cat. 12260
pMD2.G	Origene Technologies	Cat. 12259
Software and algorithms		
Thermo Xcalibur (version 2.2)	Thermo Scientific	Cat. OPTON-30965
MetaboAnalyst (version 5.0)	Pang et al.[55]	https://www.metaboanalyst.ca/
Simca (version 17)	Umetrics	https://www.sartorius.com/en/products/process-analytical-technology/data-analytics-software/mvda-software/simca

(*Continued on next page*)

Continued

REAGENT or RESOURCE	SOURCE	IDENTIFIER
OPLS-DA	N/A	https://www.creative-proteomics.com/services/opls-da-service.htm
FastQC	N/A	http://www.bioinformatics.babraham.ac.uk/projects/fastqc
HISAT2	N/A	https://daehwankimlab.github.io/hisat2/
StringTie	N/A	https://github.com/gpertea/stringtie
Ballgown	N/A	http://bioconductor.org/packages/release/bioc/html/ballgown.html
KEGG database	N/A	https://www.genome.jp/kegg/pathway.html
MSigDB databases	Broad institute	https://www.gsea-msigdb.org/gsea/msigdb
ClusterProfiler	N/A	https://bioconductor.org/packages/release/bioc/html/clusterProfiler.html
Cytoscape 3.7.2	N/A	http://cytoscape.org/
R and R Studio	N/A	http://www.r-project.org/
FlowJo 9.9.6	NIH	FlowJo
GraphPad Prism (version 9)	NIH	https://www.graphpad.com/
Image Studio	Li-Cor Biosciences	N/A
Other		
Lymphocyte Separation Medium	MP Biomedicals	Cat. 0850494
Human $CD4^+$ T Cell Isolation Kit	Miltenyi Biotec	Cat. 130-096-533
NucleoSpin RNA Kit	Macherey-Nagel	Cat. 740955
First-strand Synthesis SuperMix	Invitrogen	Cat. 11752250
FastStart Essential DNA Green Master Mix	Roche Life Science	Cat. 06924204001
miRNeasy Micro Kit	Qiagen	Cat. 217084
TruSeq Stranded Total RNA HT Kit	Illumina	Cat. 20020595
Accell siRNA delivery media	Horizon Discovery	Cat. B-005000-100
Polyjet *In Vitro* DNA Transfection Reagent	Signagen Laboratories	Cat. SL100688

RESOURCE AVAILABILITY

Lead contact

Further information and requests for resources or reagents should be directed to and will be fulfilled by the lead contact, Michael N. Sack (sackm@nih.gov). Laboratory of Mitochondrial Biology and Metabolism, NHLBI, NIH, Bldg. 10-CRC, Room 5–3342, 10 Center Drive, Bethesda, MD 20892, USA.

Materials availability

This study did not generate new unique reagents.

Data and code availability

- All data associated with this study are present in the paper or supplemental information. The RNA-seq data (Tables S1, S2, and S3) was deposited in the GEO database and the metabolomics data (Table S4) in Mendeley database. The accession number and link for the datasets are listed in the key resources table.
- This paper does not report original code.
- Any additional information required to reanalyze the data reported in this paper is available from the lead contact upon request.

EXPERIMENTAL MODEL AND SUBJECT DETAILS

Study design and human subjects

Blood from healthy volunteers for the initial vehicle versus NR supplementation studies and for initial flow cytometry and gene expression analysis and subsequent functional validation of pathways uncovered in the control vs. psoriasis cohorts (described below) were

obtained from subjects that consented to enroll on a Disease Discovery Protocol (NCT01143454). Psoriasis subjects with mild to moderate severity were then recruited at NIH Clinical Center and provided consent, on and the NHLBI IRB approved protocol (ClinicalTrials.gov registration number NCT01934660, n=12). As controls, male and age-matched healthy volunteers were recruited (n=12) through the healthy blood donor population from a Disease Discovery Protocol (NCT01143454). The average age for both the patients with Psoriasis and healthy donors was 57 years old and they were all males. The characteristic of healthy and psoriatic subjects is described in Figure 1B.

Clinical protocol of placebo/NR study

The Placebo and NR pilot study was registered in ClinicalTrials.gov with the registration number NCT02812238, approved by NHLBI IRB, and performed at the National Institutes of Health (NIH) Clinical Center. We recruited 25 subjects with an average age of 24 and average body mass index (BMI) of 23. Healthy volunteers were screened prior to signing consent and subjects were then randomly assigned to a 7-day supplementation of either NR (500 mg bid) or a matching placebo. The study protocol has been described previously for the study of monocytes,[18] and a schematic of the blood draw protocol and immune function studies is shown in Figures S7A and S7B. The blood from healthy volunteers for functional study and metabolomic analysis were obtained from subjects that consented to enroll on the Disease Discovery Protocol (NCT01143454) and from the NIH Clinical Center blood bank (NCT00001846).

METHOD DETAILS

Flow cytometry immunophenotyping

A 17-color antibody panel was designed to enable immunophenotyping of the predominant cell populations found in PBMCs and $CD4^+$ T cells (Table S5). PBMCs were thawed in FACS buffer (PBS with 0.25 mM EDTA and 0.1% BSA) with nuclease (Sigma) and $CD4^+$ T cells were isolated from healthy volunteers. The cells were activated with Cell stimulation cocktail plus protein transport inhibitors (eBioscience) and PMA (500 ng/ml, Sigma) for 4 hrs. The antibodies were listed in Table S5 followed by LIVE/DEAD Fixable Yellow stain (Invitrogen). Data were acquired with FACSymphony (BD) and post-acquisition analysis was performed using Flowjo 9.9.6 (Treestar Inc.). Analysis excluded debris and doublets using light scatter measurements, and dead cells by live/dead stain. Gating strategies used to identify immune cell subsets are provided in Table S6 and Figure S8. Briefly, the cells were first gated for singlets (FSC-H vs. FSC-A) and further analyzed for their uptake of the Live/Dead Yellow stain to determine live versus dead cells in $CD4^+$ T. Their expression of surface markers (CD25 and HLA-DR) and intracellular markers (Transcription factors and cytokines) is then determined within this gated population. Statistical significance between two groups was determined using a two-tailed Student's t-test.

Human $CD4^+$ T cell Isolation and cytokine assay

Primary peripheral blood mononuclear cells (PBMCs) were isolated from human blood by density centrifugation using Lymphocyte Separation Medium (MP Biomedicals). $CD4^+$ T cells were negatively selected from PBMCs using the $CD4^+$ T Cell Isolation Kit (Miltenyi Biotec) and cultured in RPMI 1640 media supplemented with 25 mM HEPES, 10% heat-inactivated FBS, and Penicillin/Streptomycin. Human $CD4^+$ T cells (3×10^5/well in 96-well plate) were activated with plate-coated αCD3 (5 μg/ml, BioLegend) and αCD28 (10 μg/ml, BioLegend) for 3 days in the presence of 10% autologous serum from the subjects and 5% FBS. Also, $CD4^+$ T cells (2×10^5/well in 96-well plate) were differentiated into three T cell subtypes by incubation with the specific supplements for T_H1 (20 ng/ml IL-12 and 10 μg/ml αIL-4), T_H2 (10 ng/ml IL-4 and 10 μg/ml αIFNγ) or T_H17 (20 ng/ml IL-6, 2 ng/ml TGF-β1, 10 ng/ml IL-1β, 10 ng/ml IL-23, 10 μg/ml αIL-4, and 10 μg/ml αIFNγ), respectively. They were differentiated for 3 days on plate-coated αCD3 and αCD28 in the presence of 10% autologous serum from the subjects and 5% FBS. All recombinant proteins and antibodies for differentiation media were purchased from Peprotech and eBioscience. Supernatants were collected, centrifuged to remove cells and debris, and stored at -80°C. The levels of cytokines, including IFNγ, IL-5, and IL-17 were measured by ELISA (R&D Systems). Results were normalized to cell number using the CyQuant cell proliferation assay (Invitrogen) or BCA protein assay (Pierce).

RNA sequencing and bioinformatics analysis

Total RNA from $CD4^+$ T cells was extracted with the miRNeasy Micro Kit (Qiagen) and RNA quality and integrity was assessed by Qubit 3.0 fluorometer (Thermo Fisher Scientific) and Agilent Bioanalyzer (Agilent Technologies). Libraries were prepared using TruSeq stranded Total RNA HT kit (Illumina) and sequenced in a HISeq 3000 (Illumina) by the DNA Sequencing and Genomics Core at NHLBI. FastQC (http://www.bioinformatics.babraham.ac.uk/projects/fastqc) was used to confirm quality of RNA seq fasta files. Adaptor trimming, RNA sequence alignment, gene expression quantification, and differential expression analysis was performed as previously described.[37] Genes with p value < 0.05 were considered differentially expressed (DE) genes. Pathway enrichment analysis was performed using the R package clusterProfiler[56] on DE genes that were subset into upregulated and downregulated based on the fold change values. Additional pathway inferences were made by performing pathway enrichment using the KEGG database and one of the molecular signature databases (MSigDB) collection C7 immunologic signature database (Broad institute) in R (https://www.R-project.org/). Previously published protein-protein interaction (PPI) networks between the gene of interest were extracted from the String protein database[55] and the gene nodes in the PPI network were colored red and blue for up and

downregulated genes open-source software Cytoscape.[57] The pathway enrichment plots and heatmaps were generated using ggplot2 (Wickham H (2016). *ggplot2: Elegant Graphics for Data Analysis*. Springer-Verlag New York. ISBN 978-3-319-24277-4) library in R.

Inhibitors, siRNAs, and lentiviruses

NR (0.5 mM from ChromaDex) and L-Arginine (5 mM from Sigma) were incubated for 3 days during TCR activation was used prior to the subsequent assays. PARPs inhibitor Rucaparib camsylate (Sigma) and CD38 inhibitor Compound-78c (Selleckchem) were used in cell culture at 10 μM, 20 μM, or 10 μM for 12 hrs., respectively. NRF2 inhibitor (10 μM ML385 from Selleckchem) or activator (10 μM DMF from Selleckchem), was used for overnight incubation before harvesting the cells.

For knockdown experiments, SMARTpool Accell siRNA was utilized targeting oxidative stress-related genes (NRF2, SQSTM1, GCLC, GCLM, GSR), and NAD-related genes (CD38, SARM1) (Horizon Discovery). Accell siRNA was transfected with Accell siRNA delivery media according to manufacturer's instruction (Horizon Discovery). The cells (4×10^6) with 1.5 μM siRNA were activated with plate-coated αCD3 (BioLegend) and αCD28 (BioLegend) for 3 days before assay.

To produce lentivirus, pLenti vector, pLenti-NRF2 with Myc-DDK tag, or pLenti-SQSTM1 with Myc-DDK (Origene Technologies) and packing plasmids (psPAX2 and pMD2.G from Addgene) were transfected into 293T cells using Polyjet reagent (Signagen Laboratories). Supernatants were collected 48 hours after transfection, filtered through a 0.45 μm syringe filter and concentrated by ultracentrifugation (Beckman) at 25,000 rpm for 2 hours. Virus was introduced into the $CD4^+$ T cell culture media in the presence of 8 μg/ml of DEAE-dextran (Sigma) and incubated in the presence of 50 ng/ml IL-2 for 24 hours before TCR activation.

RNA Isolation and Quantitative PCR analysis

Total RNA was extracted using NucleoSpin RNA kit (Macherey-Nagel) and cDNA was synthesized with the SuperScript III First-Strand Synthesis System for RT-PCR (Thermo Fisher Scientific). Quantitative real-time PCR was performed using FastStart Universal SYBR Green Master (Roche) and run on LightCycler 96 Systems (Roche). The primers of canonical transcription factors (TFs) of $CD4^+$ T cell were made by Integrated DNA Technologies and the sequences of the primers are listed; TBX21 (F: CGTGACTG CCTACCAGAAT and R: ATCTCCCCCAAGGAATTGAC), GATA3 (F: GAACCGGCCCCTCATTAAG and R: ATTTTTCGGTTTCTGGT CTGGAT), RORC (F: GCATGTCCCGAGATGCTGTC and R: CTGGGAGCCCCAAGGTGTAG), and EF1α (F: GTTGATATGGT TCCTGGCAAGC and R: GCCAGCTCCAGCAGCCTTC). The transcript levels of other targets were measured using validated gene-specific QuantiTech primers (Qiagen, Table S7). Relative gene expression was quantified by normalizing cycle threshold values with 18S rRNA or EF1α using the $2^{-\Delta\Delta Ct}$ cycle threshold method.

Western Blotting

Human monocytes were lysed using RIPA buffer supplemented with protease inhibitor cocktail (Roche) and phosphatase inhibitors (Pierce). Lysates were separated by NuPAGE 4-12% Bis-Tris Protein Gels (Thermo Fisher Scientific) and transferred to nitrocellulose membranes (Trans-Blot Turbo Transfer System (Bio-Rad Laboratories). Membranes were blocked with Odyssey Blocking Buffer (Li-Cor) and incubated with appropriate antibodies overnight at 4°C. Antibodies were purchased from Cell Signaling Technologies (NRF2, SQSTM1/p62, KEAP1, NQO1), and Millipore (Actin). The secondary antibody conjugated with IRDye 800CW or IRDye 680RD (Li-Cor) were then incubated for 1 hour at room temperature. Immunoblots were scanned using an Odyssey Clx imaging system (Li-Cor Biosciences). Protein band intensity was quantified using Image studio software (version 5.2) and normalized to Actin level.

Intracellular ROS and mitochondrial ROS assay

ROS (Reactive oxygen species) generation in the form of superoxide was measured also by a FACS- and microplate reader-based assay using DCFDA (2',7'-Dichlorofluorescin Diacetate, Sigma) for intracellular ROS and MitoSOX red mitochondrial superoxide indicator (Invitrogen) for mitochondrial ROS. $CD4^+$ T cells ($4\text{-}8\times10^5$ per well) were incubated with 10 μM DCFDA or 5 μM MitoSOX red in HBSS medium for 30 minutes at 37°C. Cells were subsequently washed with HBSS, and the fluorescence intensities of each subset/cell were measured by flow cytometry and microplate reader (ROS: 488 nm excitation/535 nm emission and MitoSOX red: 510 nm excitation/580 nm emission excitation). Results were normalized using the BCA protein assay (Pierce) and CyQuant cell proliferation assay (Invitrogen).

4-hydroxynonenal (4-HNE) is a product of lipid peroxidation and is employed as a stable marker for oxidative stress. 4-HNE adduct in 2×10^5 $CD4^+$ T cells was quantified by Lipid Peroxidation (4-HNE) Assay Kit (Abcam).

The total free radical presence of $CD4^+$ T cells (10-50 μg) was measured using OxiSelect *in vitro* ROS/RNS (reactive nitrogen species) assay kit (Cell Biolabs). The assay employs a proprietary quenched fluorogenic probe, dichlorodihydrofluorescin DiOxyQ (DCFH-DiOxyQ), which is a specific ROS/RNS probe that is based on similar chemistry to the popular DCFDA. ROS and RNS species can react with prepared DCFH probe, which is rapidly oxidized to the highly fluorescent DCF. Samples were measured fluorometrically against a DCF standard by microplate reader at 480 nm excitation/530 nm emission. Results were normalized to protein concentration using the BCA protein assay (Pierce).

Trolox equivalent antioxidant capacity assay

Trolox equivalent antioxidant capacity of NR was carried out using the procedure described in the antioxidant assay kit (Sigma). The principle of the antioxidant assay is formation of a ferryl myoglobin radical from metmyoglobin and hydrogen peroxide, which oxidizes the ABTS (2,2¢-azino-bis(3-ethylbenzthiazoline-6-sulfonic acid) to produce a scavenge ABTS radicals, a soluble chromogen that is green in color and can be determined spectrophotometrically at 405 nm. The absorbance was plotted as a function of the antioxidant capacity relative to the Trolox standard according to the assay protocol. The sample from each subject was analyzed in duplicate and the results were normalized to protein concentration using the BCA protein assay (Pierce).

Glutathione (GSH) measurement

GSH level was detected in 4×10^6 $CD4^+$ T cells using GSH/GSSG ratio detection assay kit (Abcam) and GSH assay kit (BioAssay Systems). Results were normalized to protein concentration using the BCA protein assay (Pierce).

NRF2 activation assay

The nuclear extracts were prepared from $CD4^+$ T cells using a nuclear extraction kit (Abcam) and quantified using BCA protein assay (Pierce). The protein specifically bound to the specific double stranded DNA sequence containing the NRF2 consensus binding site within the core antioxidant response element (ARE) (5' – GTCACAGTGACTCAGCAGAATCTG – 3') provided in the NRF2 Transcription Factor Assay Kit (Abcam). NRF2 was detected by a primary antibody that recognizes an epitope of NRF2 accessible only when the protein is activated and bound to its target DNA. NRF2 activation was measured as a colorimetric readout at OD 450 nm.

Fumarate assay

Fumarate level from $CD4^+$ T cells (1×10^6) was measured by Fumarate Assay Kit (Sigma) which results in a colorimetric (450 nm) product, proportional to the fumarate present.

Metabolomics and Data Analysis

Human $CD4^+$ T cells isolated from healthy volunteers were supplemented with 0.5mM NR or vehicle control and activated with plate-coated αCD3 and αCD28 for 3 days. Also, $CD4^+$ T cells were differentiated into Th17 for 3 days on plate-coated αCD3 and αCD28. Males with an average age of 24 years were recruited (n=10) through the healthy blood donor population of the Disease Discovery Protocol (NCT01143454). Cells pellets were collected and snap frozen in liquid nitrogen and processed using LC-MS as previously described.[18] Metabolite abundance was normalized to protein content. SIMCA software (version 15; Umetrics) was used to perform orthogonal partial least squares discriminant analysis (OPLS-DA) of metabolomic data from all 4 groups and identify variable importance in prediction (VIP) metabolites to discriminate NR vs. Vehicle. Pathway analysis of VIP metabolites was performed using MetaboAnalyst 5.0 (metaboanalyst.ca).

The polar metabolites in serum samples in the *in-vivo* placebo vs. NR supplementation study were measured using targeted MS/MS as described here. Serum samples were extracted using a standard methanol-chloroform-water extraction and reconstituted in 10 mM ammonium acetate containing internal standards at a concentration of 10 μM: proline, valine-D_8, leucine-D_{10}, lysine-U-^{13}C, glutamic acid-^{13}C, phenylalanine-D_5, succinic acid-D_3, and serotonin-D_4. Reverse-phase analysis was performed with an ACE Excel 2 C18 PFP (100A. 150 x 2.1 mm 5μm) column conditioned at 30°C. The mobile phase consisted of: (A) 0.1% formic acid in water and (B) 0.1% formic acid in acetonitrile. All solvents were analytical grade or HPLC-MS quality and sourced from Sigma-Aldrich. Targeted MS/MS was performed with a Thermo Scientific Vanquish UHPLC+ coupled to a TSQ Quantiva mass spectrometer (Thermo Fisher Scientific). The electrospray ionization source was operated in positive ionization mode at 3500 V and negative ionization mode at 2500 V. 48 mTorr nitrogen at 420°C was used for solvent evaporation. Data acquisition and processing were performed using Thermo Xcalibur software (version 2.2; Thermo Scientific). Peak intensity was normalized to appropriate internal standards.

Statistical analysis

Statistical analysis was performed using Prism 7 software (GraphPad) and results are represented as mean ± s.e.m. unless otherwise indicated. Comparisons of two groups were calculated using paired or unpaired two-tailed Student's *t*-test. One-way ANOVA was used to measure statistical differences in more than 2 groups. Two-way ANOVA was used if there were two nominal variables in addition to a measurement variable. For all tests, $p < 0.05$ was considered significant. For *in vivo* and *in vitro* studies, n represents the number of biological replicates per group and is reported in Figure Legends.

ADDITIONAL RESOURCES

Clinical Study NCT01934660: https://classic.clinicaltrials.gov/ct2/show/NCT01934660, Clinical Study NCT02812238: https://classic.clinicaltrials.gov/ct2/show/NCT02812238, Clinical Study NCT01143454: https://classic.clinicaltrials.gov/ct2/show/NCT01143454, Clinical Study NCT00001846: https://classic.clinicaltrials.gov/ct2/show/NCT00001846.